AD-A059 694 NAVAL POSTGRADUATE SCHOOL MONTEREY CALIF F/G 13/1
THE ENHANCEMENT OF HEAT TRANSFER IN A ROTATING HEAT PIPE.(U)
JUN 78 I S PURNOMO

UNCLASSIFIED NL

1 OF 2
ADA
059694

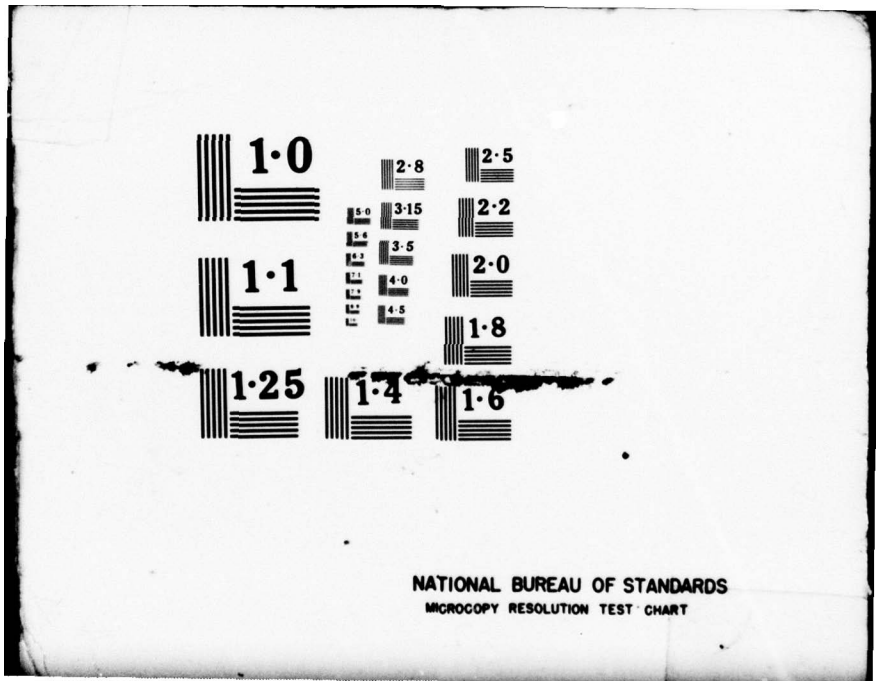
1·0
1·1
1·25
2·8
3·15
3·5
4·0
4·5
1·4
2·5
2·2
2·0
1·8
1·6
NATIONAL BUREAU OF STANDARDS
MICROCOPY RESOLUTION TEST CHART

LEVEL II

(2)

NAVAL POSTGRADUATE SCHOOL
Monterey, California

THESIS

(6) THE ENHANCEMENT OF HEAT TRANSFER
IN
A ROTATING HEAT PIPE.

by

(9) Master's thesis,

(10) Ignatius Slamet/Purnomo

(11) June 1978 (12) 110p.

Thesis Advisor: P.J. Marto

Approved for public release; distribution unlimited.

UNCLASSIFIED

SECURITY CLASSIFICATION OF THIS PAGE (When Date Entered)

REPORT DOCUMENTATION PAGE		READ INSTRUCTIONS BEFORE COMPLETING FORM
1. REPORT NUMBER	2. GOVT ACCESSION NO.	3. RECIPIENT'S CATALOG NUMBER
4. TITLE (and Subtitle) The Enhancement of Heat Transfer in a Rotating Heat Pipe		5. TYPE OF REPORT & PERIOD COVERED Engineer's Thesis; June 1978 6. PERFORMING ORG. REPORT NUMBER
7. AUTHOR(s) Ignatius Slamet Purnomo		8. CONTRACT OR GRANT NUMBER(s)
9. PERFORMING ORGANIZATION NAME AND ADDRESS Naval Postgraduate School Monterey, California 93940		10. PROGRAM ELEMENT, PROJECT, TASK AREA & WORK UNIT NUMBERS
11. CONTROLLING OFFICE NAME AND ADDRESS Naval Postgraduate School Monterey, California 93940		12. REPORT DATE June 1978 13. NUMBER OF PAGES 109
14. MONITORING AGENCY NAME & ADDRESS(if different from Controlling Office)		15. SECURITY CLASS. (of this report) 15a. DECLASSIFICATION/DOWNGRADING SCHEDULE

16. DISTRIBUTION STATEMENT (of this Report)

Approved for public release; distribution unlimited.

17. DISTRIBUTION STATEMENT (of the abstract entered in Block 20, if different from Report)

18. SUPPLEMENTARY NOTES

19. KEY WORDS (Continue on reverse side if necessary and identify by block number)

Heat Transfer

20. ABSTRACT (Continue on reverse side if necessary and identify by block number)

A linear triangular finite element formulation was used to solve the steady state two dimensional conduction heat transfer equation. A FORTRAN IV computer program of the above formulation, employing double precision arithmetic and compact storage techniques, was applied to study heat transfer in an internally finned rotating heat pipe. Results were obtained for water in a copper and stainless

DD FORM 1 JAN 73 1473 EDITION OF 1 NOV 65 IS OBSOLETE
S/N 0102-014-6601 |

UNCLASSIFIED
SECURITY CLASSIFICATION OF THIS PAGE (When Date Entered)

(20. ABSTRACT Continued)

steel condenser with varying outside heat transfer coefficient, rotational speed, and fin angle (number of fins).

Numerical results of the heat transfer rate in the copper condenser were shown to have less than 2% variance to those obtained earlier. A rotating heat pipe designed to operate with a small value of outside heat transfer coefficient experiences no significant increase of the heat transfer rate with an increase in rotational speed, since the value of the outside thermal resistance dominates.

Heat transfer rate continuously increases as the fin angle decreases. However, the increase is only slight when the fin angle is less than 11 degrees.

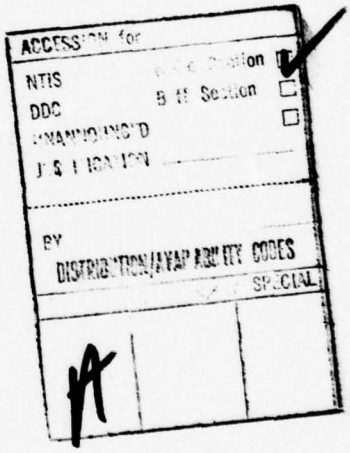

Approved for public release; distribution unlimited.

The Enhancement of Heat Transfer in A Rotating Heat Pipe

by

Ignatius Slamet Purnomo
Major Artillery, Republic Indonesian Army

Submitted in partial fulfillment of the requirements for the degrees of

MASTER OF SCIENCE IN MECHANICAL ENGINEERING

and

MECHANICAL ENGINEER

from the

NAVAL POSTGRADUATE SCHOOL

June 1978

Author _____

Approved by: _____
Thesis Advisor

_____
Thesis Advisor

_____
Chairman, Department of Mechanical Engineering

_____
Dean of Science and Engineering

ABSTRACT

A linear triangular finite element formulation was used to solve the steady state two dimensional conduction heat transfer equation. A FORTRAN IV computer program of the above formulation, employing double precision arithmetic and compact storage techniques, was applied to study heat transfer in an internally finned rotating heat pipe. Results were obtained for water in a copper and stainless steel condenser with varying outside heat transfer coefficient, rotational speed, and fin angle (number of fins).

Numerical results of the heat transfer rate in the copper condenser were shown to have less than 2% variance to those obtained earlier. A rotating heat pipe designed to operate with a small value of outside heat transfer coefficient experiences no significant increase of the heat transfer rate with an increase in rotational speed, since the value of the outside thermal resistance dominates.

Heat transfer rate continuously increases as the fin angle decreases. However, the increase is only slight when the fin angle is less than 11 degrees.

TABLE OF CONTENTS

LIST OF TABLES

LIST OF FIGURES

TABLE OF SYMBOLS

A	cross sectional area for flow in ft^2; finite element area
b	height of the fin in ft; finite element factor
c	sonic speed in ft/sec; finite element factor
g	acceleration of gravity in ft/hr^2
h	convective heat transfer coefficient in $Btu/hr\text{-}ft^2\text{-}F$
h_{fg}	latent heat of vaporization in Btu/lbm
k_f	thermal conductivity of condensate film in Btu/hr-ft-F
k_w	thermal conductivity of condenser wall in Btu/hr-ft-F
L	finite element sides
M	mass flow rate of condensate in lbm/hr
N	two dimensional linear shape function
P	pressure of the vapor in lbf/ft^2
Q	heat transfer rate in Btu/hr
R	internal radius of condenser in ft; thermal resistance in hr-F/Btu
T	temperature
U	velocity of liquid in ft/sec
X Y	axis of Cartesian system coordinate
x	coordinate measuring distance along the condenser length
y	coordinate measuring distance vertically from fin surface
z	coordinate measuring distance along fin surface

GREEK

α	fin half angle in degrees
δ	condensate film thickness in ft

ε local trough width in ft

ϕ condenser half cone angle in degrees

ρ_e density of the liquid in lbm/ft^3

ρ_v density of the vapor in lbm/ft^3

σ surface tension of the liquid in lbf/ft

μ_ℓ viscosity of the liquid in lbm/ft-sec

μ_v viscosity of the vapor in lbm/ft-sec

ω angular velocity rad/sec

ACKNOWLEDGMENTS

The author wishes to express his appreciation to Dr. P.J. Marto, Professor of Mechanical Engineering, and Dr. David Salinas, Associate Professor of Mechanical Engineering, for their advice and guidance throughout the course of the development of this thesis. Without their perseverance and assistance this work could not have been accomplished.

Finally the author wishes to thank his wife, Ignatia Murwani, for her understanding and encouragement throughout the course of this study.

I. INTRODUCTION

A. THE ROTATING HEAT PIPE

The rotating heat pipe is a closed container designed to transfer a large amount of heat in rotating machinery. Its three main component parts are: a cylindrical evaporator, a truncated cone condenser, and a working fluid as shown in Figure 1.

At rotation above the critical speed of a rotating heat pipe, the working fluid forms an annulus in the evaporator, and will be vaporized by heat addition in it. The vapor flows toward the condenser, as a result of a pressure difference, transporting the latent heat of evaporation with it. External cooling of the condenser causes the vapor on the inner wall to condense and release its latent heat of evaporation. The centrifugal force due to the rotation has a component acting along the condenser wall that will act to drive the condensate back to the evaporator where the cycle is repeated.

In a conventional heat pipe, the force driving the condensate back to the evaporator is due to capillary action, which poses a limit to its operation. However, the driving force in the rotating heat pipe can be designed to operate in any orientation, including in a zero gravity field.

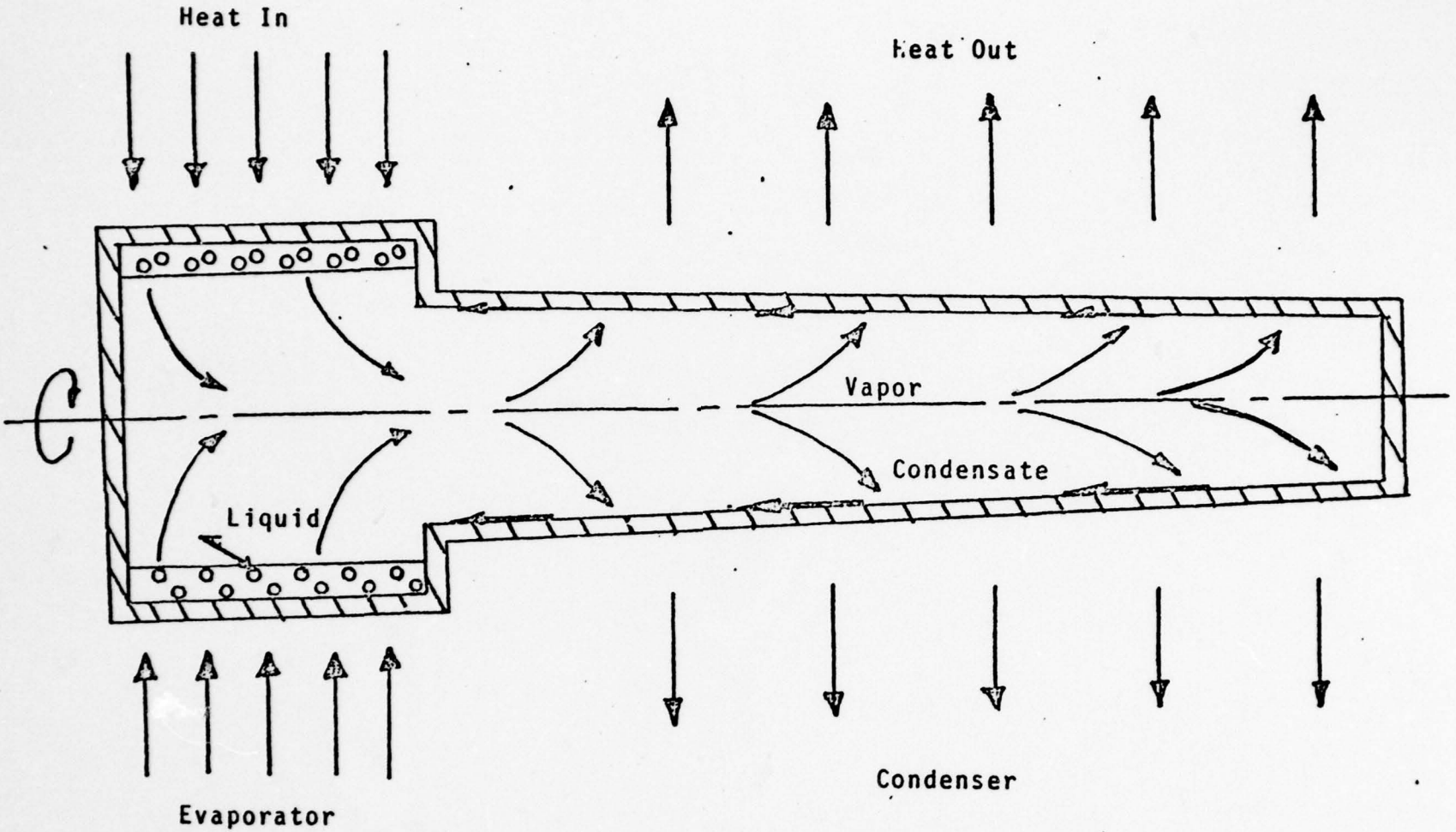

Figure 1 Schematic Drawing of a Rotating Heat Pipe

B. UTILIZATION OF AN INTERNALLY FINNED CONDENSER

The first theoretical investigation of the rotating heat pipe conducted at the Naval Postgraduate School, was performed by Ballback [1] in 1969. He studied the limitations of performance imposed on the rotating heat pipe due to various fluid dynamic mechanisms. Using existing theory and experimental correlations, he was able to estimate the sonic limit, boiling limit, entrainment limit, and the condensing limit of performance.

1. The Sonic Limit

When increasing the heat flux in a rotating heat pipe, it is entirely conceivable to reach a limiting flow rate of the vapor brought on by a choked flow condition in the pipe. This condition imposes a limiting value on the amount of energy the vapor can transport, thus reducing the effectiveness of the heat pipe. Since the heat transfer method in the rotating heat pipe depends strongly on the latent energy of the working fluid, the rate of heat transfer in the heat pipe can be expressed as:

$$Q_t = \dot{m}_v h_{fg} \qquad \text{(I-1)}$$

where $\dot{m}_v$ = vapor mass flow rate in lbm/hr. From the continuity equation,

$$\dot{m}_v = \rho_v U_v A \qquad \text{(I-2)}$$

where

U_v = velocity of the vapor in ft/sec, and

A = cross sectional area for the vapor flow in ft^2.

The heat transfer rate becomes

$$Q_t = \rho_v U_v A h_{fg} \qquad \text{(I-3)}$$

and the vapor velocity is considered to be sonic,

$$U_v = c = \sqrt{g_0 kRT} \qquad \text{(I-4)}$$

where

c = sonic velocity in ft/sec

g_0 = gravitational constant = 32.1739 ft-lbm/lbf-sec^2

k = ratio of specific heats

R = gas constant in ft-lbf/lbm R, and

T = absolute temperature in °R.

2. Boiling Limit

It has been postulated by Kutateladze [2] that the transition from nucleate to film boiling is totally a hydrodynamic process. With this postulation, he determined the theoretical formula for predicting the burnout heat flux:

$$Q_t = K\sqrt{\rho_v}\, A_b\, h_{fg}\{\sigma\, g(\rho_f - \rho_v)\}^{1/4} \qquad \text{(I-5)}$$

where

K = constant value

ρ_v = density of the vapor in lbm/ft^3

A_b = heat transfer area in the boiler in ft^2

h_{fg} = latent heat of vaporization in Btu/lbm

σ = surface tension in lbf/ft

g = acceleration of gravity in ft/hr^2

ρ_f = density of fluid in lbm/ft^3

The experimental data obtained by Kutateladze suggested a value for K in the range of 0.13 to 0.19.

3. Entrainment Limit

The flooding constraint in a wickless heat pipe was examined by Sakhuja [3], who assumed that:

a) The vapor and liquid are exposed to each other in a counterflow movement.

b) The counterflowing vapor tends to retard the falling film of liquid through shear stress.

c) The liquid film remains stable and smooth, and the shear stress is usually small.

d) The buoyancy forces resulting from the density difference between the vapor and liquid are the means for maintaining the counterflow.

e) The buoyancy forces are balanced by dissipative effects which are proportional to the momentum fluxes of vapor and liquid streams.

His resulting correlation for flooding is

$$Q_t = \frac{A_x C^2 h_{fg} \sqrt{gD(\rho_f - \rho_v)\rho_v}}{[1 + (\rho_v/\rho_f)^{1/4}]^2} \qquad \text{(I-6)}$$

where

Q_t = heat transfer rate in Btu/hr

A_x = flow area in ft^2

C = dimensionless constant, 0.725 for tube with sharp edged flange

h_{fg} = latent heat of vaporization in Btu/lbm

g = acceleration due to gravity in ft/hr^2

D = inside diameter of heat pipe in ft

ρ_f = density of the fluid in lbm/ft^3

ρ_v = density of the vapor in lbm/ft^3

4. Condensing Limit

Ballback [1] determined the condensation solution for a rotating heat pipe by modeling the condenser section of a rotating heat pipe as a rotating truncated cone, from which the following condensation limit was developed:

$$Q_t = \pi\left\{\frac{2}{3}\frac{k_f \rho_f \omega^2 h_{fg}[T_s - T_w]^3}{\mu_f \sin^2\phi}\right\}^{\frac{1}{4}} \{[R_o + L\sin\phi]^{\frac{8}{3}} - R_o^{\frac{8}{3}}\}^{\frac{3}{4}} \qquad \text{(I-7)}$$

where

Q_t = total heat transfer rate in Btu/hr

k_f = thermal conductivity of the condensate film in Btu/hr-ft-F

ρ_f = density of fluid in lbm/ft^3

ω = angular velocity in 1/hr

h_{fg} = latent heat of vaporization in Btu/lbm

T_s = saturation temperature in F

T_w = inside wall temperature in F

μ_f = viscosity of fluid in lbm/ft-hr

ϕ = half cone angle in degrees

R_o = minimum wall radius in ft

L = length along the wall of the condenser in ft

The condensing limit equation is a function of the geometry and speed of the rotating heat pipe, and the physical properties of the working fluid.

Tantrakul [4] calculated these limitations on a heat pipe with specific physical characteristics as shown in Table 1, with the results shown in Figure 2.

TABLE 1

Specification of a Typical Rotating Heat Pipe

Length	14.000	inches
Minimum diameter	2.000	inches
Wall thickness	0.125	inches
Internal half angle	1.000	degree
Rotating speed	2700	RPM

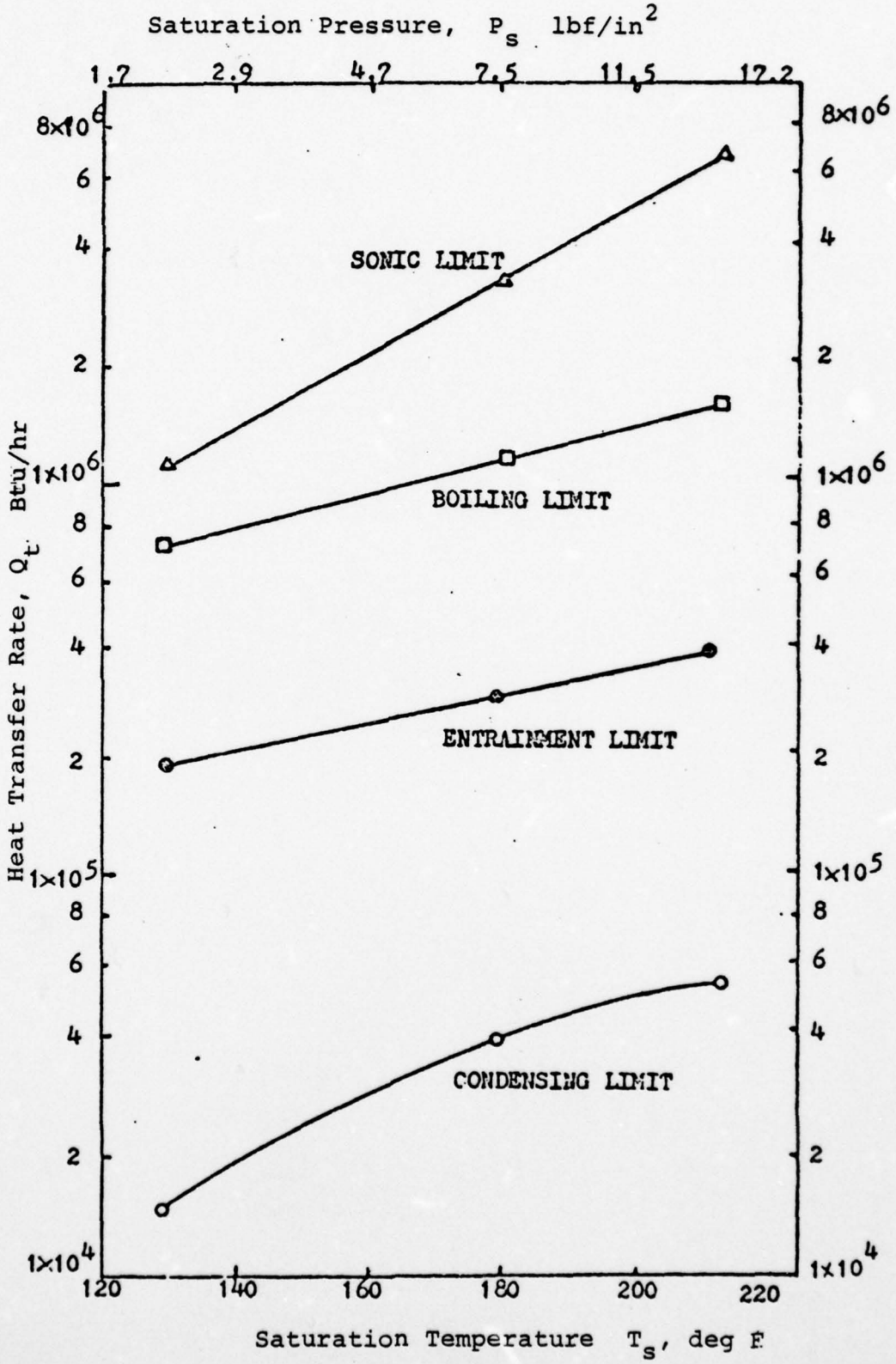

Figure 2 Operating Limits of a Typical, Water-filled, Rotating Heat Pipe

Obviously from the results in Figure 2, the condensing limit line is the predominant limitation for the amount of heat that can be transferred from the heat pipe. However, the other limitations may become important as the heat pipe geometry and operating conditions are varied.

In order to augment the heat transfer capacity of the heat pipe, the current efforts are aimed at raising the condensing limit line which may be accomplished by:

a) a high value of cone angle, to increase the driving force.

b) some type of promoter of dropwise condensation to increase the value of the convective heat transfer coefficient, h.

c) use of an internally finned condenser to increase the inner wall surface area and the value of h, since the presence of the fin will decrease the condensate film thickness.

By machining fins in the inner wall of the condenser, a significant improvement of heat transfer will be realized.

C. ANALYSIS OF THE INTERNALLY FINNED ROTATING HEAT PIPE

A disadvantage of improving the performance of a rotating heat pipe with fins machined in the inner wall is that an increase in the wall thermal resistance results due to the increase in wall thickness brought on by the fins. By using a material with a high value of thermal conductivity, this effect can be minimized.

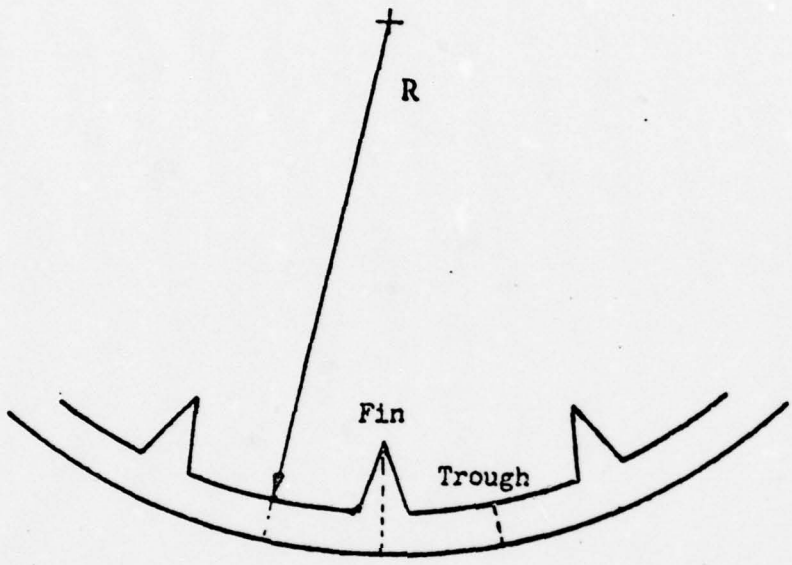

Figure 3 Internally Finned Condenser Geometry Showing Fins, Troughs and Lines of Symmetry

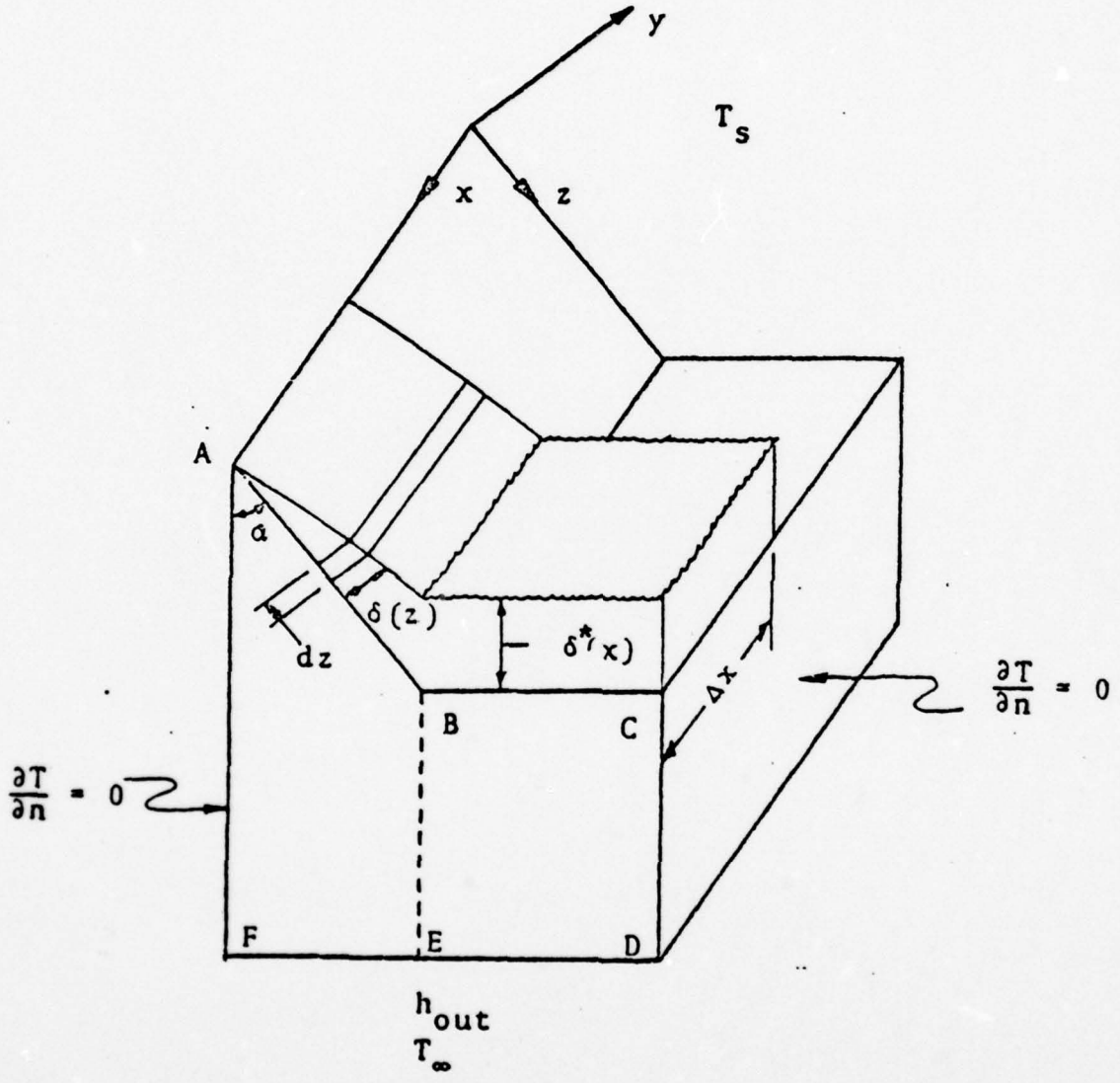

Figure 4 Internally Finned Condenser Geometry Considered in Analysis of Schafer [5]

Schafer [5] developed an analytical model for the case of fins with a triangular profile as shown in Figures 3 and 4. In the analysis he assumed one dimensional heat conduction through the wall. Corley [6] for this same case developed a two dimensional heat conduction model using a Finite Element Method, and also assumed a parabolic temperature distribution along the fin surface. His results indicated a significant improvement in heat transfer performance of about 75%, above that predicted by the one dimensional model of Schafer [5]. However, Corley [6] cautiously noted a probable error of 50% existed in the calculation of the heat transfer at the fin apex, and consequently mentioned that there may be a total heat transfer error of as high as 15%. Also, he noted that his analysis was not valid fro a stainless steel condenser because of numerical difficulties. Tantrakul [4] modified Corley's computer program by increasing the number of finite elements in order to minimize the apex heat transfer error. His results with this modification converged with the results of Corley.

D. THESIS OBJECTIVES

The objectives of this thesis are:

1. To generate a general computer program for two dimensional steady state Conduction Heat Transfer.
2. To use this program to study heat transfer in a finned rotating heat pipe.

3. To conduct a parametric study for a proposed heat pipe design.

II. FINITE ELEMENT SOLUTION

A. REVIEW OF THE PREVIOUS ANALYSIS

Schafer [5] studied the one dimensional model heat transfer solution and Corley [6] studied the two dimensional model for an internally finned rotating heat pipe. Both used the same assumptions and boundary conditions based upon the analysis of Ballback [1], which are similar to those used in the Nusselt analysis of film condensation on a flat wall. The more important of those assumptions are:

1. steady state operation
2. film condensation, as opposed to dropwise condensation
3. laminar condensate flow along both the fin and the trough
4. static balance of forces within the condensate
5. one dimensional conduction heat transfer through the film thickness (no convective heat transfer in the condensate film)
6. no liquid - vapor interfacial shear forces
7. no condensate subcooling
8. zero heat flux boundary conditions on both sides of the wall section (symmetry conditions), as shown in Figures 5 and 6
9. saturation temperature at the fin apex
10. zero film thickness at the fin apex
11. negligible curvature of the wall

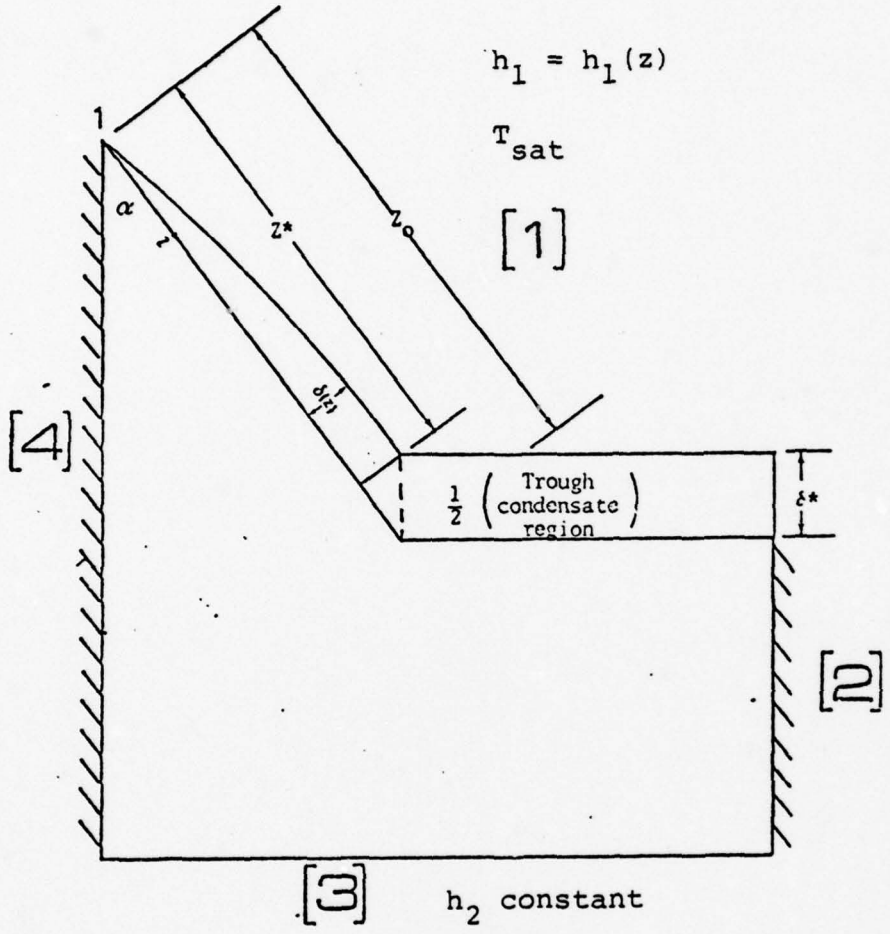

$$\frac{\partial^2 T}{\partial x^2} + \frac{\partial^2 T}{\partial y^2} = 0$$

b.c.

a) $T_1 = T_{sat}$

b) $-k \frac{\partial T}{\partial n} = h_1 (T - T_{sat})$ in region [1]

c) $-k \frac{\partial T}{\partial n} = h_2 (T - T_\infty)$ in region [3]

d) $\frac{\partial T}{\partial n} = 0$ in region [2] and [4]

Figure 5 Differential Equation and Boundary Conditions Considered in Analysis of Corley [6]

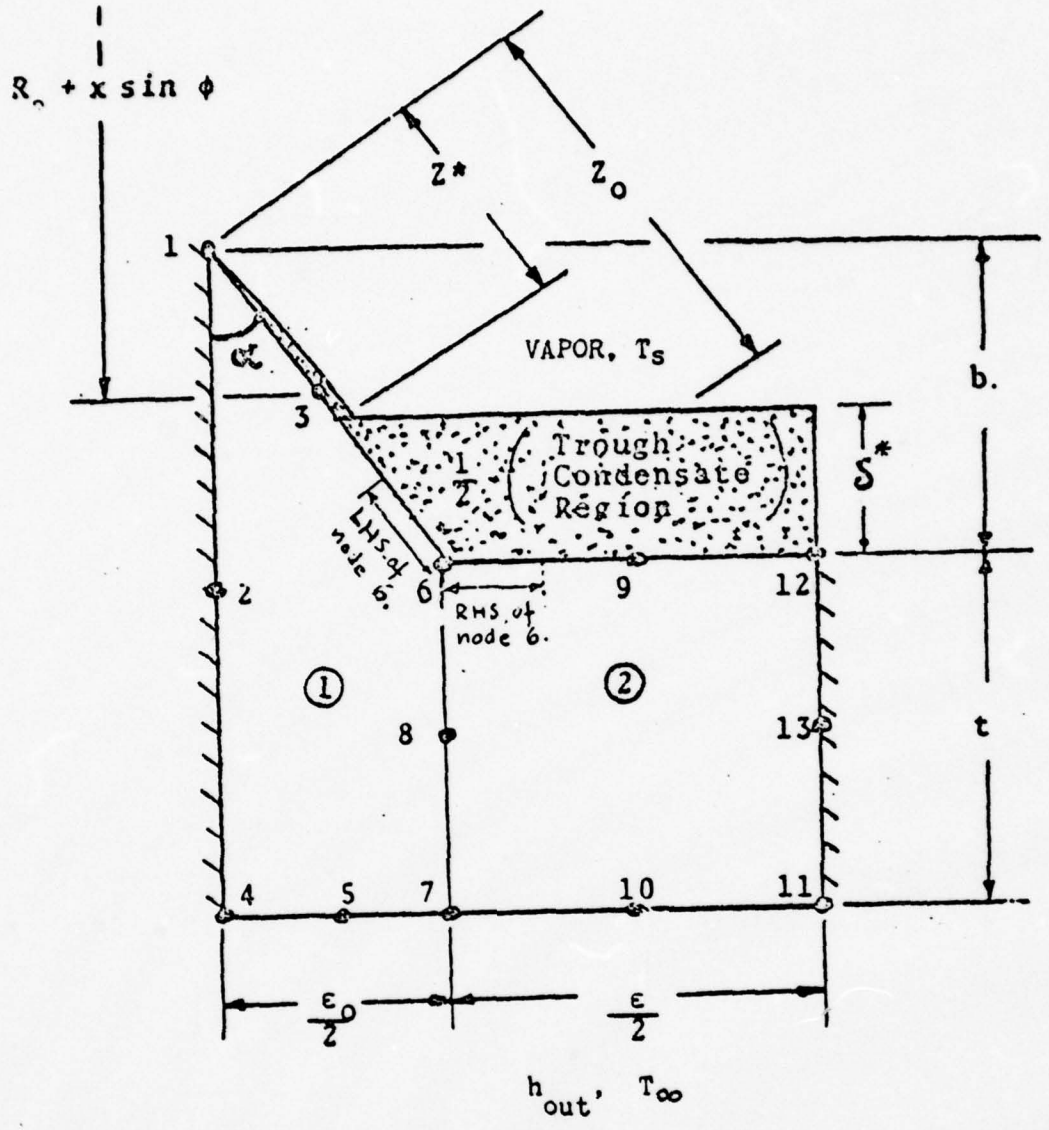

t = 0.03125 in.
b = 0.025 in.
R = 0.762 in.
ϕ = 1°

Figure 6 Internally Finned Condenser Finite Element Geometry Considered in Analysis of Corley [6]

The complete development of Schafer's finned condenser heat transfer is presented in his thesis. His results are used as a comparison in this thesis.

However, since the same fluid flow and heat transfer theory applies to the two dimensional conduction model, Corley [6] utilized this model and further developed it using the Finite Element Method. He considered an internally finned geometry as shown in Figure 6, and used the fin condensate film equation derived by Schafer [5]

$$\delta^3(z)d\delta(z) = \frac{k_f(T_S-T_w(z))\ \mu_f\ dz}{\rho_f^2\ \omega^2(R_0 + x \sin \phi)\ h_{fg} \cos \phi \cos \alpha} \qquad \text{(II-1)}$$

where

δ = the fin condensate film thickness in ft

k_f = thermal conductivity of working fluid in Btu/hr-ft-F

ρ_f = density of working fluid in lbm/ft^3

μ_f = viscosity of working fluid in lbm/ft-hr

ω = angular velocity in 1/hr

R_0 = minimum radius in ft

x = distance along apex of fin in ft

Z = distance along the fin, from the apex in ft

ϕ = half cone angle in degrees

h_{fg} = latent heat of vaporization in Btu/lbm

He assumed a parabolic temperature distribution along the fin surface,

$$T_w(z) = r_1 z^2 + s_1 z + t_1 \qquad \text{(II-2)}$$

to calculate the convective heat transfer coefficient along the fin surface. He developed a solution of the steady state two dimensional conduction heat transfer equation:

$$\nabla k \cdot \nabla T = 0 \qquad \text{(II-3)}$$

with boundary conditions as shown in Figure 5

a) saturation temperature at the apex,

$$T = T_{sat}$$

b) convective boundary condition in region [1]

$$-k \frac{\partial T}{\partial n} = h_1 (T - T_{sat}), \quad \text{and in region [3]}$$

$$-k \frac{\partial T}{\partial n} = h_2 (T - t_\infty).$$

c) symmetry conditions, $\frac{\partial T}{\partial n} = 0$, in region [2] and region [4].

He used the 8 node quadratic isoparametric element in the mesh shown in Figure 6, and a modification of the three dimensional isoparametric Finite Element Method computer program assembled by Lew [7].

Applying the boundary condition a), $T = T_{sat}$ at $z = 0$ gives $t_1 = T_{sat}$ and equation (II-2) becomes:

$$T_w(z) = r_1 z^2 + s_1 z + T_{sat}, \qquad \text{(II-4)}$$

or

$$T_{sat} - T_w(z) = -r_1 z^2 - s_1 z. \qquad \text{(II-5)}$$

Upon substituting equation (II-5) into equation (II-2), and integrating the result from z = 0 to z, gives an equation for $\delta(z)$:

$$\delta(z) = \left[\frac{4\, k_f(-r_1 \frac{z^3}{3} - s_1 \frac{z^2}{2})\mu_f}{\rho_f^2\, \omega^2 (R_0 + x \sin\phi)\, h_{fg} \cos\phi \cos\alpha}\right]^{1/4}. \qquad \text{(II-6)}$$

Assuming one dimensional conduction heat transfer through the thin condensate film, the local convective heat transfer coefficient is:

$$h(z)_{fin} = \frac{k_f}{\delta(z)} = \left[\frac{k_f^3\, \rho_f^2\, \omega^2 (R_0 + x\sin\phi) h_{fg} \cos\phi \cos\alpha}{4\, \mu_f (-r_1 \frac{z^3}{3} - s_1 \frac{z^2}{2})}\right]^{1/4} \qquad \text{(II-7)}$$

where k_f = fluid thermal conductivity in Btu/hr-ft-F which is applicable from z = 0 to $z = Z^* = Z_0 - \delta^*/\cos\alpha$; where δ^* is the trough condensate film thickness, as shown in Figure 5. Across the width of the trough, the convective heat transfer coefficient is:

$$h(x)_{trough} = \frac{k_f}{\delta^*(x)} \qquad \text{(II-8)}$$

The heat transfer rate for the entire condenser is then determined within the computer program algorithm by dividing its axial length into 100 increments of length Δx (see Figure 4), and solving for the incremental heat transfer rate using an iterative procedure. The incremental rates are then summed to yield the total heat transfer rate.

Figure 7 shows a flow chart description of the computer program used in Corley's analysis [6]. Constant values of r_1 and s_1 are determined at each increment using Lagrangian interpolation fit of the temperature at the nodes 1, 3, and 6 (see Figure 6) from the previous iteration. At the first increment, values of r_1 and s_1 are calculated from an initial guess of the temperature at these nodes. The average nodal values of h_{1avg}, h_{3avg} and the average of h of the left hand boundary region associated with node 6 (see Figure 6), are calculated using the position dependent value $h(z)_{fin}$ (equation (II-7)) in a Simpson's Rule approximation. In the trough, $h(x)_{trough}$ is calculated from equation (II-8), using the δ^* value calculated from the previous increment, and this value is used as the average convective heat transfer coefficient for nodes 9 and 12, and the right hand boundary of node 6. The average heat transfer coefficients calculated for the left- and right-hand boundary region of node 6 are weighted by their respective region length. These values are then added to yield the average convective

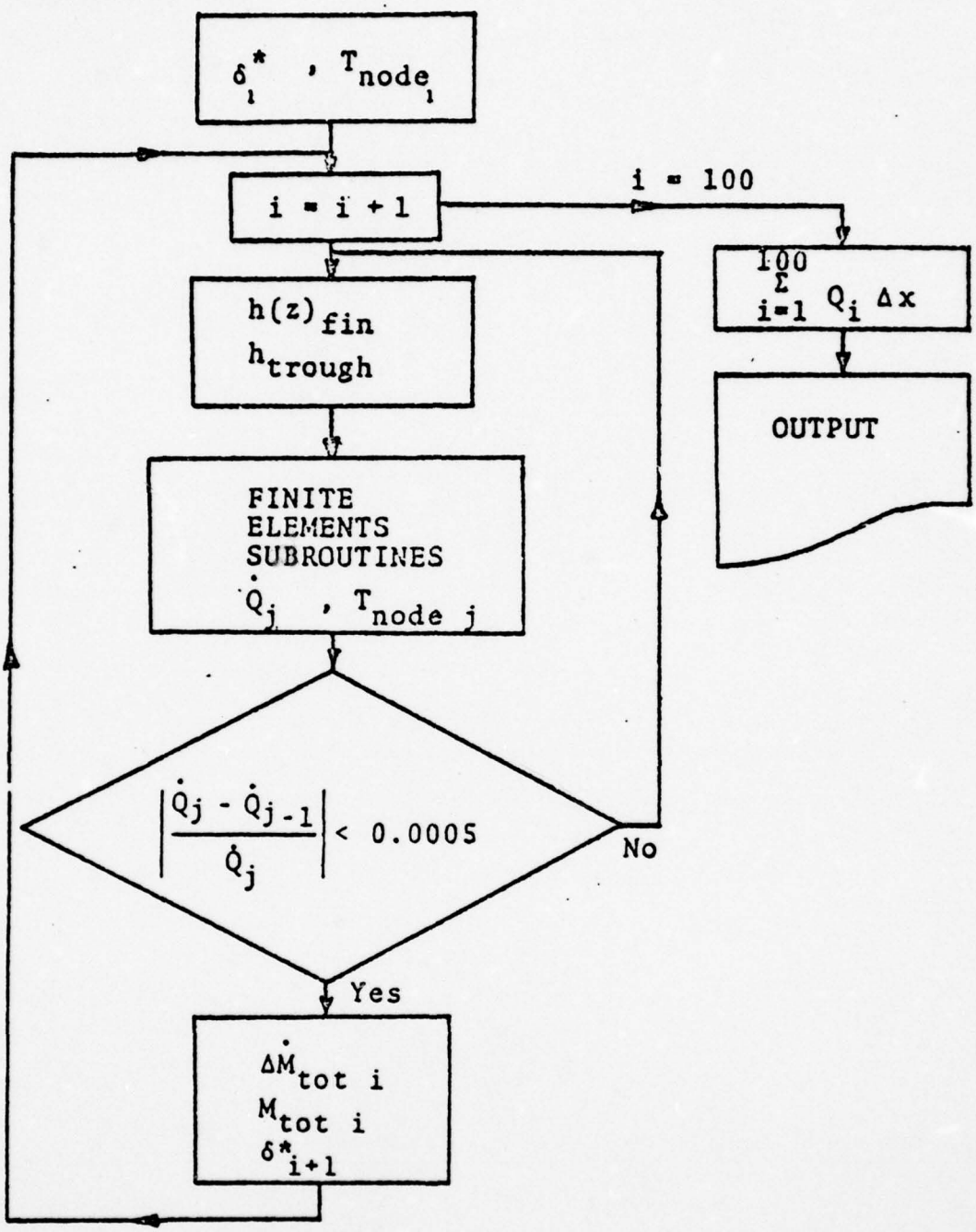

Figure 7 Computer Program Flowchart of Two Dimensional Conduction Analysis of Corley [6]

coefficient for node 6, h_{6avg}. The remaining boundary conditions are now applied, and the incremental heat transfer rate per unit of condenser length Q_i, and the nodal temperature values are generated from the Finite Element Method subroutine. If the resultant heat transfer rate converges to within a 0.05% change from the value of the previous iteration, i.e.

$$\left|\frac{Q_j - Q_{j-1}}{Q_j}\right| \leq 0.0005 \qquad \text{(II-9)}$$

then the increment is deemed solved and Q_i is set equal to the final iteration, Q_j. However, if the convergence criterion is not met, newly calculated nodal temperature values are used to establish a new set of inner wall convective heat transfer coefficients, and the Finite Element solution is repeated until the heat transfer rate converges to within 0.0005 tolerance. The incremental mass flow rate in the trough is now calculated using the relation

$$\dot{M}_{tot\ i} = 2\frac{Q_i}{h_{fg}}\Delta x \qquad \text{(II-10)}$$

where this value is added to the mass flow from the previous increments. A modification of the trough mass flow rate equation from Schafer's thesis [5] is used to calculate the subsequent interval's trough condensate thickness $\delta^*(x)$, with the polynomial root finder subroutine:

$$\dot{M}_{tot}(x) = \frac{\rho^2 \omega^2 (R_0 + x\sin\phi)\delta^*(x)^2 \sin\phi}{3\mu_f}[\delta^*(x)\varepsilon+\delta^*(x)^2\tan\alpha] \qquad \text{(II-11)}$$

This incrementation is continued until the entire length of the condenser is transversed. Incremental heat transfer rates are summed, hence the total heat transfer rate:

$$Q_{tot} = 2 N_{fin} \sum_{i=1}^{100} (Q_i \Delta x) \qquad \text{(II-12)}$$

where N_{fin} is the number of fins along the inner wall circumference.

To start the incrementation, two initial guesses are made. These are the initial value of δ^* which is taken from the analysis by Sparrow and Gregg for condensation on a rotating disk [8] and the initial values of the temperatures at the nodes 1, 3 and 6.

Corley [6] noted that an error of 50% due to calculation of heat transfer rate at the apex may cause a total error of 15%. To minimize this error he suggested an increase in the number of finite elements.

Tantrakul [4] continued Corley's study. He increased the number of finite elements between the apex of the fin and the trough as shown in Figures 8 and 9. To save computer execution time, he reduced the number of increments to 25 instead of 100 increments as in Corley's calculation. However, even with the reduced number of increments, the

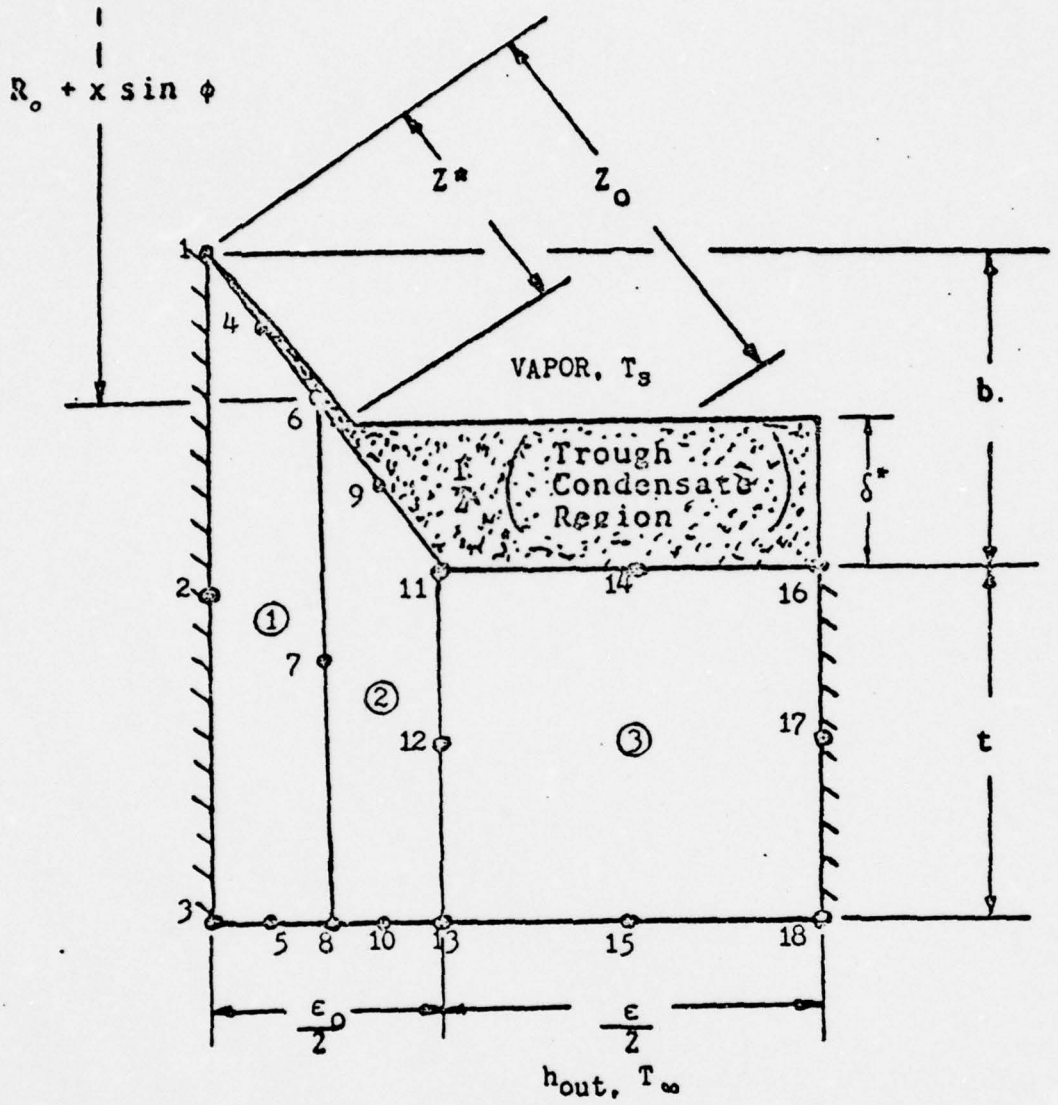

t = 0.03125 in.
b = 0.025 in.
R_o = 0.762 in.
ϕ = 1°

Figure 8 Internally Finned Condenser Finite Element Geometry (3 Finite Elements) Considered in Analysis of Tantrakul [4]

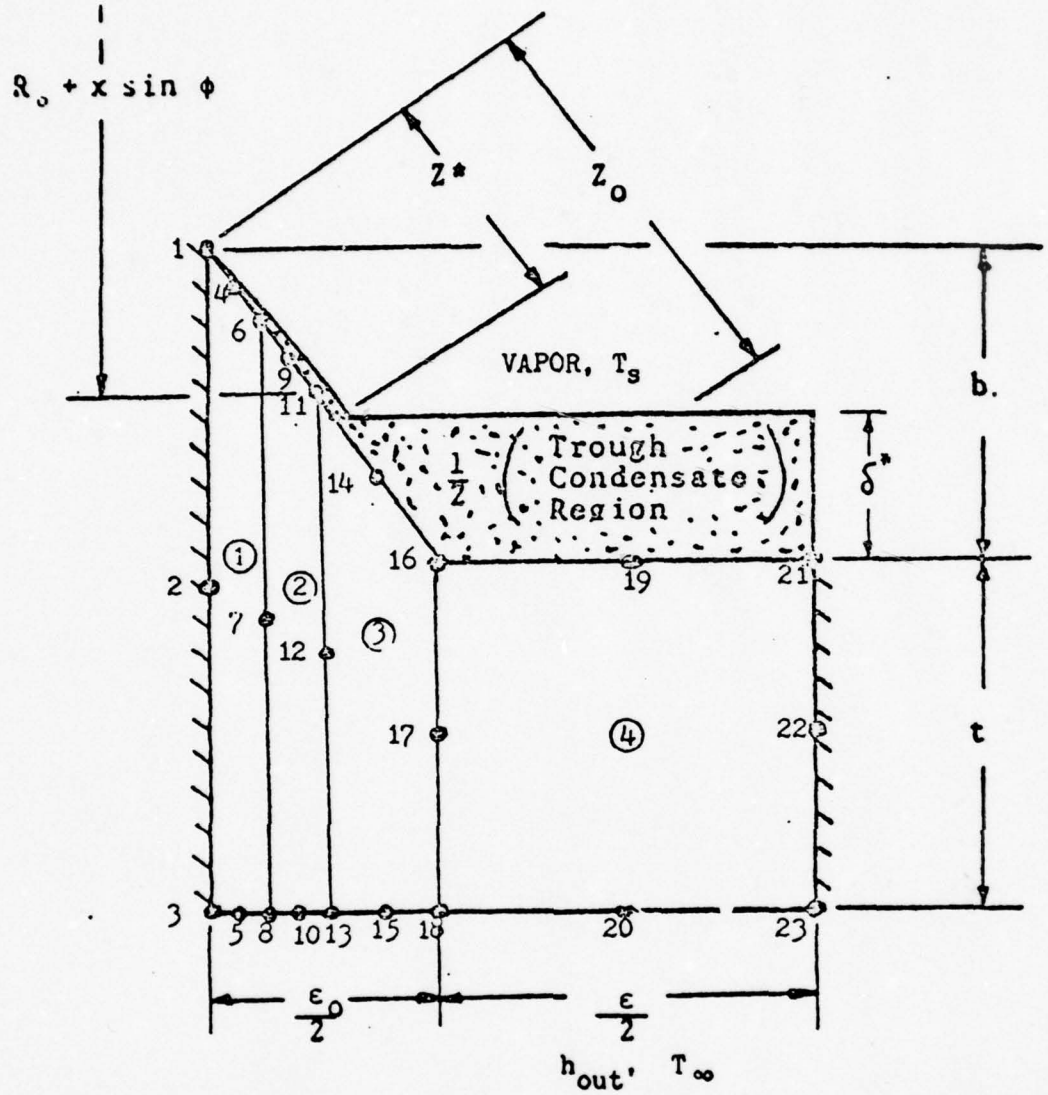

t = 0.03125 in.
b = 0.025 in.
R_o = 0.762 in.
ϕ = 1°.

Figure 9 Internally Finned Condenser Finite Element Geometry (4 Finite Elements) Considered in Analysis of Tantrakul [4]

results of Tantrakul [4] converged favorably with Corley's results [6].

B. FORMULATION

In this thesis the author used the same physical relation and technique to calculate the heat transfer rate from the condenser. These are listed below:

a) assume parabolic temperature distribution along the fin boundary

b) utilize equation (II-6) to determine the condensate thickness, $\delta(z)$

c) use equation (II-9), (II-10), and (II-11) to calculate the mass flow rate in the trough, and determine the subsequent condensate thickness.

d) iterate to arrive at the desired solution with the convergence criterion 0.01, since the results are converged at this value (see Table 2).

For the Finite Element Method solution, the author used a linear triangular finite element model as shown in Figures 10 through 12.

Corley [6] solved the field equation for the fin with the following boundary conditions:

a) temperature at the apex is equal to the saturation temperature

b) convective boundary conditions in the inside and outside of the condenser

c) symmetry condition on the sides.

TABLE 2

Comparison of Theoretical Heat-Transfer Rate on a Copper Finned Condenser at 3000 RPM, for h_{out} = 5000 Btu/hr-ft^2-deg. F with a Variation of Convergence Criterion.

Fin half angle	No. of fins	T_{sat} (°F)	HEAT TRANSFER RATE (Btu/hr) CONVERGENCE CRITERION, $(Q_{j+1}-Q_j)/Q_j$				
			0.1	0.05	0.01	0.001	0.0001
10	276	100	46164.0	46164.0	46164.0	46164.0	46164.0
		150	122280.0	122280.0	122280.0	122280.0	122280.0
		200	198180.0	198180.0	198180.0	198180.0	198180.0
30	84	100	42569.0	42569.0	42569.0	42569.0	42569.0
		150	111970.0	111970.0	111970.0	111970.0	111970.0
		200	181040.0	181040.0	181040.0	181040.0	181040.0
50	40	200	165130.0	165130.0	165130.0	165130.0	165130.0

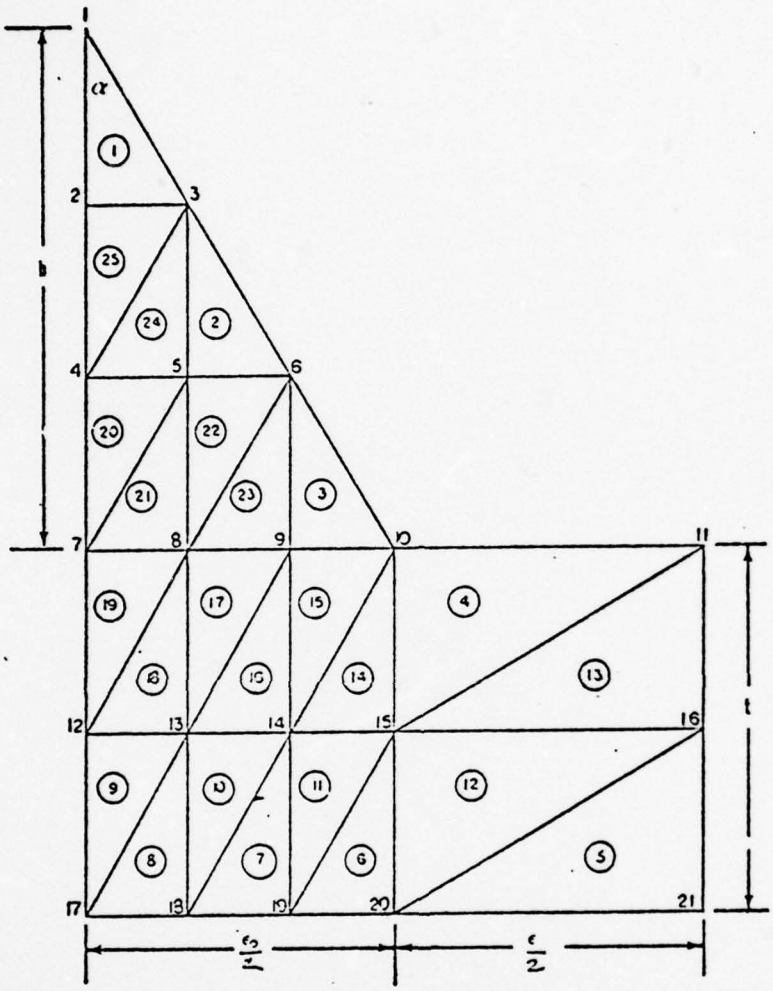

t = 0.03125 in

b = 0.025 in

R_2 = 0.762 in

$\emptyset = 1^{o}$

Figure 10 Condenser Geometry Considered with 25 Linear Triangular Finite Elements

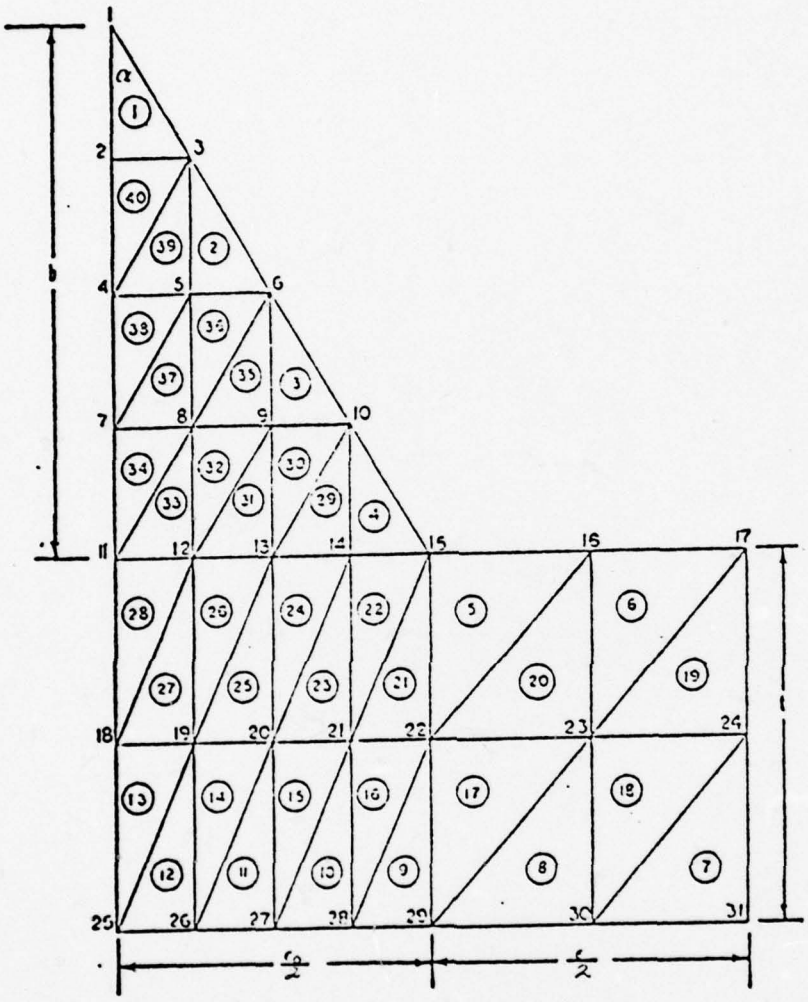

$t = 0.03125$ in.

$b = 0.025$ in.

$R_2 = 0.762$ in.

$\phi = 1^{\circ}$

Figure 11 Condenser Geometry Considered with 40 Linear Triangular Finite Elements

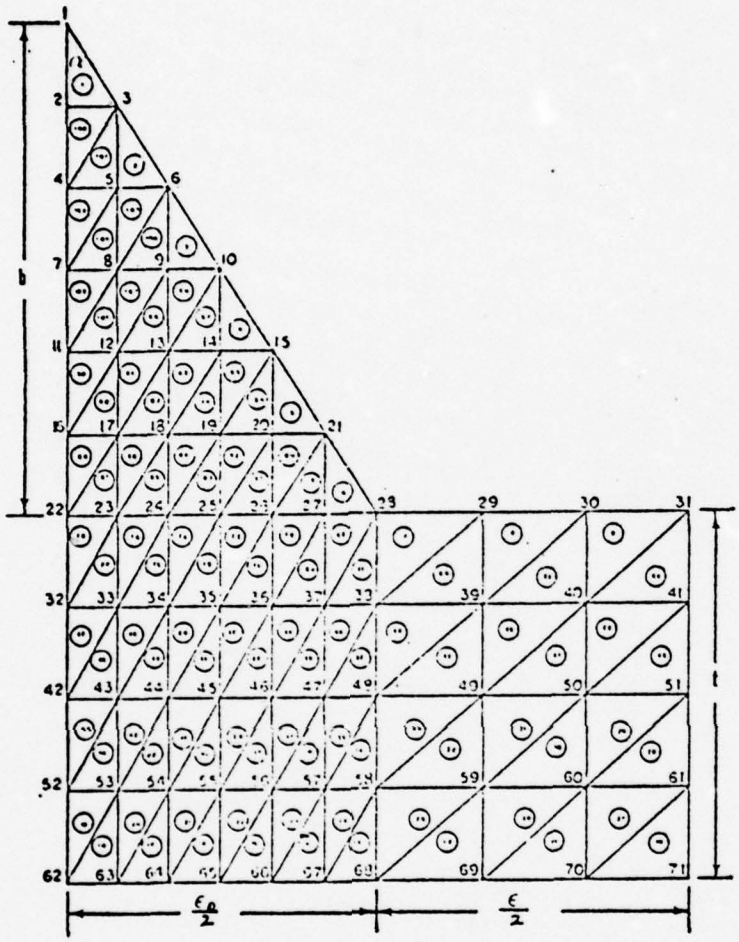

t = 0.03125 in

b = 0.025 in

R_2 = 0.762 in

Ø = 1°

Figure 12 Condenser Geometry Considered with 108 Linear Triangular Finite Elements

The first boundary condition indicates no heat transfer at the apex and a value of infinity for the convective heat transfer coefficient h. Since the value of h in reality never equals infinity, the author let the value of temperature at the apex float, which is in agreement with the theoretical analysis for the extended surface in a one dimensional case. Only for a fin with a small angle or a very long length can the temperature at the apex become equal to the environment temperature (saturation temperature in this case).

Therefore the statement of the problem for the formulation of the Finite Element Method is shown in Figure 13:

$$\frac{\partial^2 T}{\partial x^2} + \frac{\partial^2 T}{\partial y^2} = 0 \qquad \text{(II-13)}$$

with the boundary conditions:

a) in region 1, $-k \frac{\partial T}{\partial n} = h_1 (T - T_{sat})$ (II-14)

b) in region 3, $-k \frac{\partial T}{\partial n} = h_2 (T - T_\infty)$ (II-15)

c) in region 2 and 4, $\frac{\partial T}{\partial n} = 0$ (II-16)

Dividing the domain into linear triangular finite elements, the differential equation within each element is:

$$\frac{\partial^2 T^{(e)}}{\partial x^2} + \frac{\partial^2 T^{(e)}}{\partial y^2} = 0 \qquad \text{(II-17)}$$

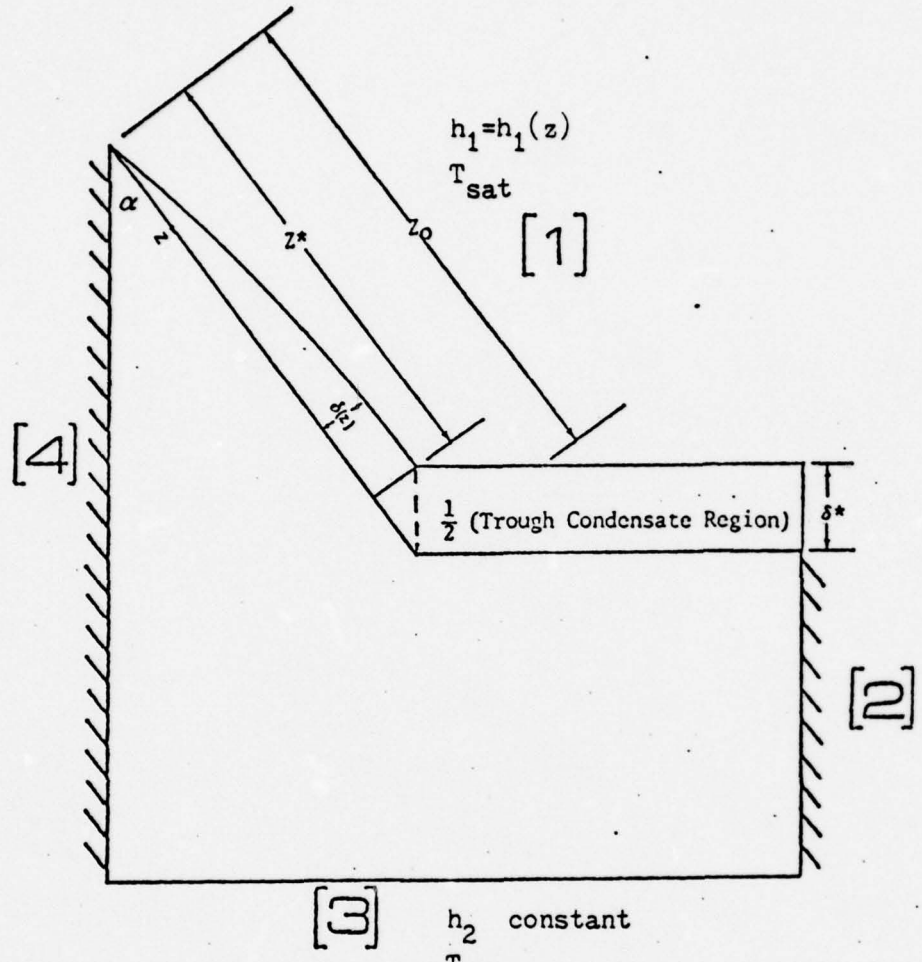

$$\frac{\partial^2 T}{\partial x^2} + \frac{\partial^2 T}{\partial y^2} = 0$$

b.c.

a) $- k \frac{\partial T}{\partial n} = h_1 (T - T_{sat})$ in region [1]

b) $- k \frac{\partial T}{\partial n} = h_2 (T - T_\infty)$ in region [3]

c) $\frac{\partial T}{\partial n} = 0$ in region [2] and [4]

Figure 13 Differential Equation and Boundary Conditions Considered in Analysis

with the boundary conditions:

$$\text{a)} \quad -k^{(e)} \frac{\partial T^{(e)}}{\partial n} = h^{(e)} (T^{(e)} - T_s^{(e)}) \qquad \text{(II-18)}$$

for elements with sides along the convective boundary, and

$$\text{b)} \quad \frac{\partial T^{(e)}}{\partial n} = 0 \qquad \text{(II-19)}$$

for others. In the above equations,

$T^{(e)}$ = temperature within the element

$k^{(e)}$ = thermal conductivity of the element; assumed to be constant

$h^{(e)}$ = convective heat transfer coefficient along the boundary of the element, assumed to be constant

$T_s^{(e)}$ = surrounding temperature at the boundary of the element.

Define the approximate value of the temperature distribution within each element as:

$$T^{(e)} \simeq T_N^{(e)}(x,y) = \sum_{i=1}^{3} N_i(x,y)\, T_i^{(e)} \qquad \text{(II-20)}$$

where

N_i = Two dimensional linear shape function, and

$T_i^{(e)}$ = nodal temperature.

Using equation (II-20), equation (II-17) can be written in approximate form as

$$R = \sum_{i=1}^{3} T_i^{(e)} \frac{\partial^2 N_i}{\partial x^2} + \sum_{i=1}^{3} T_i^{(e)} \frac{\partial^2 N_i}{\partial y^2} \qquad \text{(II-21)}$$

where

R = residual.

Applying the Galerkin criterion:

$$\int_{A^{(e)}} R\, N_j \, dA^{(e)} = 0 \qquad \text{(II-22)}$$

and substituting equation (II-21) into equation (II-22), gives:

$$\int_{A^{(e)}} \sum T_i^{(e)} \frac{\partial^2 N_i}{\partial x^2} N_j \, dA^{(e)} + \int_{A^{(e)}} \sum T_i^{(e)} \frac{\partial^2 N_i}{\partial y^2} N_j \, dA^{(e)} = 0$$

Applying Gauss' theorem to the factors on the right side yields the symmetric equation:

$$-\sum T_i^{(e)} \int_{A^{(e)}} \left(\frac{\partial N_i}{\partial x} \frac{\partial N_j}{\partial x} + \frac{\partial N_i}{\partial y} \frac{\partial N_j}{\partial y} \right) dA^{(e)}$$

$$+ \int_{L^{(e)}} N_j \frac{\partial T_i^{(e)}}{\partial n} \, dL^{(e)} = 0 \qquad \text{(II-23)}$$

where

$A^{(e)}$ = area domain, and

$L^{(e)}$ = length domain.

Substituting equation (II-18) and (II-19) into the second term of equation (II-23), gives:

$$\int_{L^{(e)}} N_j \frac{\partial T_i^{(e)}}{\partial n} dL^{(e)} = - \int_{L^{(e)}} N_j \, \phi(T^{(e)}) \, dL^{(e)} \qquad \text{(II-24)}$$

where

$$\phi(T^{(e)}) = \begin{cases} \frac{h^{(e)}}{k^{(e)}}(T^{(e)} - T_s^{(e)}) & \text{for an element with its side along the convective boundary} \\ 0 & \text{others} \end{cases}$$

Therefore equation (II-23) can be written in the form:

$$\sum_{i=1}^{3} T_i^{(e)} \int_{A^{(e)}} \left[\frac{\partial N_i}{\partial x}\frac{\partial N_j}{\partial x} + \frac{\partial N_i}{\partial y}\frac{\partial N_j}{\partial y}\right] dA^{(e)}$$

$$+ \int_{L^{(e)}} N_j \, \phi(T^{(e)}) \, dL^{(e)} = 0 \qquad \text{(II-25)}$$

The solution of

$$\int_{A^{(e)}} \left(\frac{\partial N_i \partial N_j}{\partial x \, \partial x} + \frac{\partial N_i \partial N_j}{\partial y \, \partial y} \right) dA^{(e)} = (p_{ij})^{(e)} \qquad \text{(II-26)}$$

where

$$p_{ij} = \frac{b_i b_j}{4A^{(e)}} + \frac{c_i c_j}{4A^{(e)}} \qquad \text{(II-27)}$$

$$b_i = Y_j - Y_k \qquad \text{(II-28)}$$

$$c_i = X_k - X_j \qquad \text{(II-29)}$$

$$\left.\begin{matrix} i \\ j \\ k \end{matrix}\right\} = 1, 2, 3$$

as shown in Figure 14. Recalling equation (II-24), for elements with an edge along a convective boundary,

$$\int_{L^{(e)}} N_j \phi(T^{(e)}) dL^{(e)} = T_i^{(e)} \frac{h^{(e)}}{k^{(e)}} \int_{L^{(e)}} N_i N_j \, dL^{(e)}$$

$$- T_s^{(e)} \frac{h^{(e)}}{k^{(e)}} \int_{L^{(e)}} N_j \, dL^{(e)} \qquad \text{(II-30)}$$

Applying equation (II-30) for elements with the nodal point 1 and 2 located on the convective boundary, gives

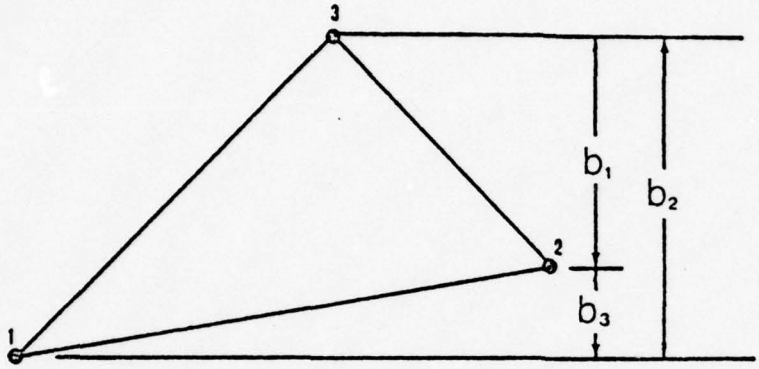

$$b_1 = Y_2 - Y_3$$
$$b_2 = Y_3 - Y_1$$
$$b_3 = Y_1 - Y_2$$

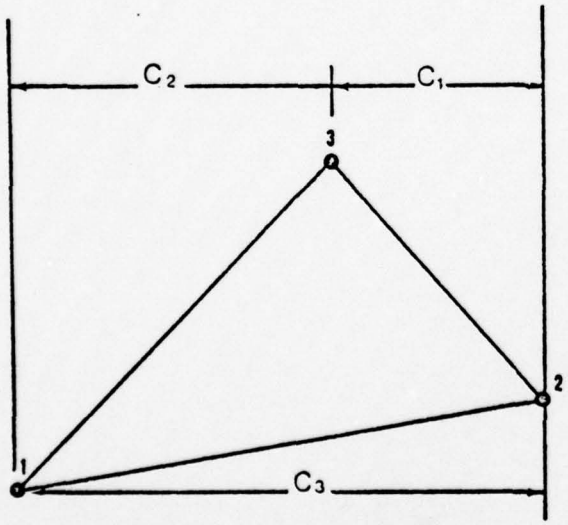

$$c_1 = X_3 - X_2$$
$$c_2 = X_1 - X_3$$
$$c_3 = X_2 - X_1$$

$$2A = |c_j b_i - c_i b_j|$$

Figure 14 Linear Triangular Finite Element Geometry

$$\int_{L^{(e)}} N_j \, \phi(T^{(e)}) \, dL^{(e)} = T_i^{(e)} \frac{h^{(e)}}{k^{(e)}} \int_{L^{(e)}} \begin{Bmatrix} \rho_1 \\ \rho_2 \\ 0 \end{Bmatrix}^{<\rho_1, \rho_2, 0>} dL^{(e)}$$

$$- T_s^{(e)} \frac{h^{(e)}}{k^{(e)}} \int_{L^{(e)}} \begin{Bmatrix} \rho_1 \\ \rho_2 \\ 0 \end{Bmatrix} dL^{(e)} \qquad \text{(II-31)}$$

where

ρ_1, ρ_2 = one dimensional linear shape function.

Therefore, equation (II-23) can be written:

$$\sum_i T_i^{(e)} \left[(p_{ij})^{(e)} + \frac{h^{(e)}}{k^{(e)}} \int_{L^{(e)}} \begin{Bmatrix} \rho_1 \\ \rho_2 \\ 0 \end{Bmatrix}^{<\rho_1, \rho_2, 0>} dL^{(e)} \right]$$

$$= \frac{h^{(e)}}{k^{(e)}} T_s^{(e)} \int_{L^{(e)}} \begin{Bmatrix} \rho_1 \\ \rho_2 \\ 0 \end{Bmatrix} dL^{(e)}$$

or

$$(K)^{(e)} \{T\}^{(e)} = \{F\}^{(e)} \qquad \text{(II-31)}$$

where

$$(K)^{(e)} = \begin{bmatrix} \frac{b_1^2+c_1^2}{4A^{(e)}} + \frac{h^{(e)}L_{21}^{(e)}}{3k^{(e)}} & \frac{b_1b_2+c_1c_2}{4A^{(e)}} + \frac{h^{(e)}L_{21}^{(e)}}{6k^{(e)}} & \frac{b_1b_3+c_1c_3}{4A^{(e)}} \\ \frac{b_1b_2+c_1c_2}{4A^{(e)}} + \frac{h^{(e)}L_{21}^{(e)}}{6k^{(e)}} & \frac{b_2^2+c_2^2}{4A^{(e)}} + \frac{h^{(e)}L_{21}^{(e)}}{3k^{(e)}} & \frac{b_2b_3+c_2c_3}{4A^{(e)}} \\ \frac{b_1b_3+c_1c_3}{4A^{(e)}} & \frac{b_2b_3+c_2c_3}{4A^{(e)}} & \frac{b_3^2+c_3^2}{4A^{(e)}} \end{bmatrix},$$

and

$$\{F\}^{(e)} = \frac{h^{(e)}\, T_s^{(e)}\, L_{21}^{(e)}}{k^{(e)}} \begin{Bmatrix} 1 \\ 1 \\ 0 \end{Bmatrix} .$$

The element matrix equation is then assembled into a system matrix equation with the sequencing based upon element and system nodal point connectivity.

The heat transfer rate within each element was calculated by

$$Q^{(e)} = h^{(e)}\, L_{12}^{(e)}\, \Delta x \left(\frac{T_1^{(e)} + T_2^{(e)}}{2} - T_s^{(e)} \right) \qquad \text{(II-32)}$$

where

$T_1^{(e)}$ = temperature at node 1

$T_2^{(e)}$ = temperature at node 2

$T_s^{(e)}$ = surrounding temperature

$h^{(e)}$ = convective heat transfer coefficient

$L_{21}^{(e)}$ = length between nodal points 1 and 2

as shown in Figure 15.

C. THE COMPUTER PROGRAM

The program consists of a main program and three subroutines;

a) the routine "COORD" used to define positions of system coordinate points

b) the routine "FORMAF" used to formulate the Finite Element Method equations

c) the routine "BANDEC" as an equation solver for a symmetric matrix which has been transformed into banded form.

The input data is entered with the units of inches for the length, degrees for the angle, Btu/hr-ft^2-F for convective heat transfer coefficients, and in F for the temperatures.

Input data is arranged in 6 classifications, and is shown in Table 3 .

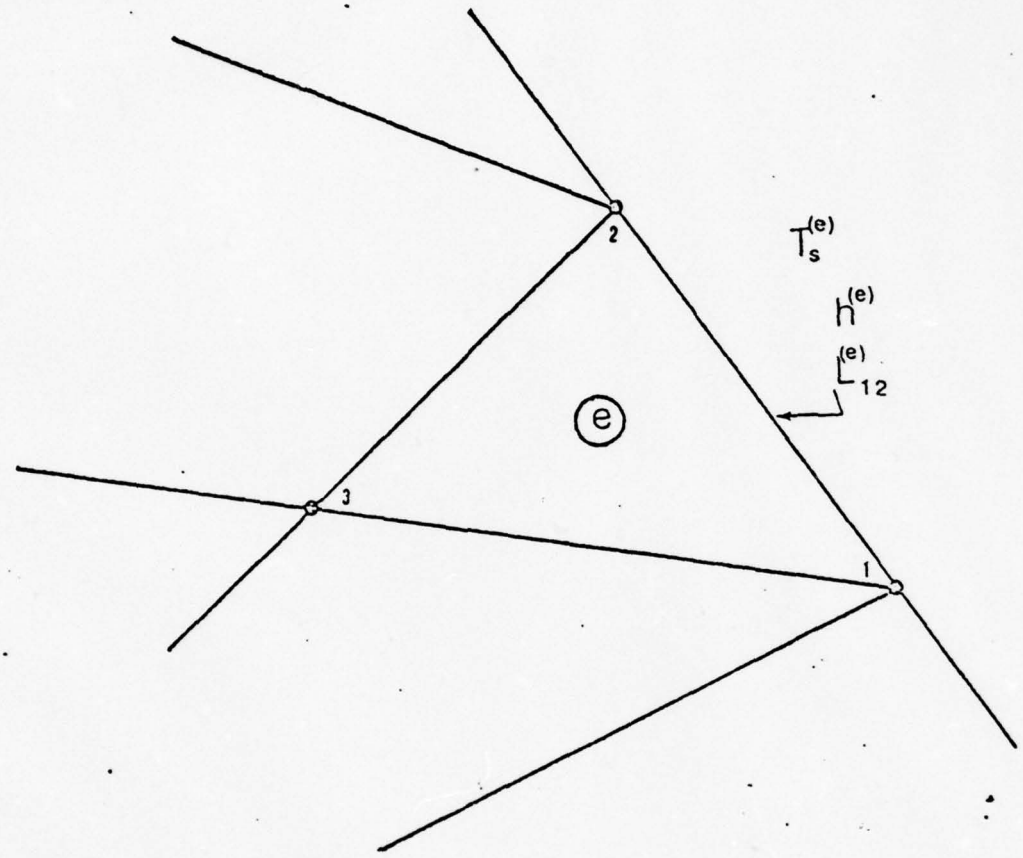

$$Q^{(e)} = h^{(e)} L_{12}^{(e)} \Delta \times \left(\frac{T_1^{(e)} + T_2^{(e)}}{2} - T_s^{(e)} \right)$$

Figure 15 · Heat Transfer Rate of an Element, $Q^{(e)}$

TABLE 3

Classification Of Input Data

Classification	Type of input data
I	system and element connectivity
II	condenser geometry
III	statement of the problem
IV	convergence criterion
V	specification to determine the system coordinate point
VI	initial guess of the temperature at the nodal points along the fin and the trough

A detailed description of each of these classifications follows:

Classification I

```
READ (5, 100) NEL, NSNP, NBAN
100 FORMAT (3I5)
```

Explanation: NEL = number of elements

NSNP = number of system nodal points

NBAN = system band width

```
READ (5, 200) (IEL,(ICOR(IEL,I),I=1,3),IEL=1,NEL)
200 FORMAT (4I5)
```

Explanation: IEL = the element number

ICOR(IEL,I) = system nodal point (NP) corresponding to NP I of element IEL

Note: - numbering the element, first for all elements with a convective boundary, starting from the top to the bottom, then others

- numbering the nodal point of an element is counterclockwise
- the elements with convective boundary have nodal point 1 and 2 located on the convective boundary

Classification II

```
READ (5, 300) CL, CANGL, RBASE, R2, THICK, BFIN
300 FORMAT ( 6G10.5)
```

Explanation:

CL = condenser length in inches

CANGL = half cone angle in degrees

RBASE = minimum radius of the condenser in inches

$R2 = RBASE + \frac{BFIN}{2}$

THICK = condenser wall thickness in inches

BFIN = the height of the fin in inches

```
READ (5, 400) NDIV, NEST, NEFB, NBOTI, NBOTF
400 FORMAT ( 5I5)
```

Explanation:

NDIV = number of increments along the length of the condenser

NEST = number of the element on the right end of the trough

NEFB = the element number with convective boundary located at the base of the fin

NBOTI = the element number with convective boundary located at the right hand of the bottom side

NBOTF = the element number with convective boundary located at the left hand of the bottom side

```
    Classification III
    READ (5, 500) (MRPM(I),I=1,3)
500 FORMAT ( 3I5 )
```

Explanation: MRPM = number of RPM (ω)

```
    READ (5, 600) (TSS(I),I=1,3)
600 FORMAT ( 3G10.5 )
```

Explanation: TSS = saturation temperature of the working fluid (T_{sat})

```
    READ (5, 700) TINF
700 FORMAT (G10.5)
```

Explanation: TINF = outside temperature (T_{∞})

```
    READ (5, 800) (HINF(I),I=1,3)
800 FORMAT ( 3G10.5 )
```

Explanation HINF = outside convective heat transfer coefficient (h_{out})

```
    Classification IV
    READ (5, 900) CRIT
900 FORMAT ( G10.5)
```

Explanation: CRIT = convergence criterion (0.01)

```
    Classification V
    READ (5, 1000) (FANGL(I),(=1,3)
1000 FORMAT ( 3G10.5 )
Explanation:     FANGL = fin half angle      (α)
    READ (5, 1100) IFF
1100 FORMAT ( I5 )
Explanation:      IFF = n-1, where n is the number of rows
                        of the upper triangular fin section
    READ (5, 1200) (KFIN(I),KFF(I),(=1,IFF)
1200 FORMAT ( 16I5 )
Explanation       KFIN = the number of system nodal points
                         located on the symmetric boundary
                         of triangular fin section, but does
                         not include the system nodal points
                         located at the base of the fin and
                         the apex
                   KFF = the number of system nodal points
                         located along the fin convective
                         boundary, but does not include the
                         system nodal points located at
                         the base of the fin and the apex
    READ (5, 1300) DOBF, DOTH, JTC, JLC, JINT, KT
1300 FORMAT ( 2G10.5, 4I5 )
Explanation:      DOBF = number of column within the fin
                  DOTH = number of column within the trough
```

JTC = number of the system nodal point located at the junction of the symmetry boundary and the line of intersection between the fin and the condenser wall

JLC = the number of the system nodal point located at the center of system coordinate

JINT = the numerical difference between the two adjacent system nodal points vertically at the condenser wall section

KT = the number of rows within the wall section

Note : as an example for 25 finite elements is shown in Figure 16

Classification VI

READ (5, 1700) T(IE)

READ (5, 1700) T(IG)

1700 FORMAT (G10.5)

Explanation: T = initial values of the temperature estimate at the nodal points 1 and 2, for elements with convective boundary along the fin and the trough

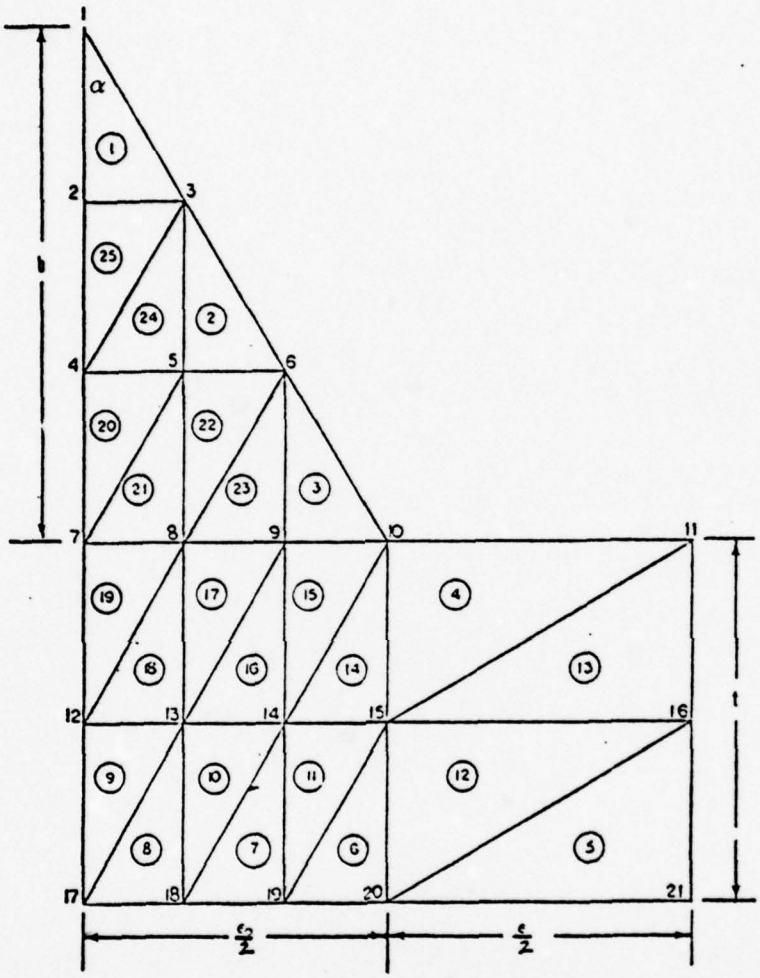

IFF = 2	DOBF = 3.0	JLC = 17
KFIN = 2 ; 4	DOTH = 1.0	JINT = 5
KFF = 3 ; 6	JTC = 7	KT = 2

Figure 16 Specification for Input Data to Determine the Coordinate of the System Nodal Points

D. TEST CASES

Before the Finite Element Method program (routine "FORMAF") was applied to the condenser problem, a series of test cases were analysed. These cases allowed a comparison to the results obtained from previous analyses and reference 9. These cases are listed below:

1. A rectangular block in a uniformly convective environment on three sides, with a specified temperature on the non-convective boundary. These results are compared with reference 9 as shown in Figure 17.
2. A rectangular block in a uniformly convective environment on the top and bottom side, insulated on the other sides. A comparison of these results with the exact values and Corley's results [6] is shown in Figure 18.
3. A rectangular block with triangular fin in a uniformly convective environment along the fin and bottom side, insulated on the wall. A comparison of the results with Corley's results is shown in Figure 19.

The results show good agreement with the results of reference 9 (case 1), and are comparable with the exact values (case 2). Therefore, "FORMAF" can be used for further applications.

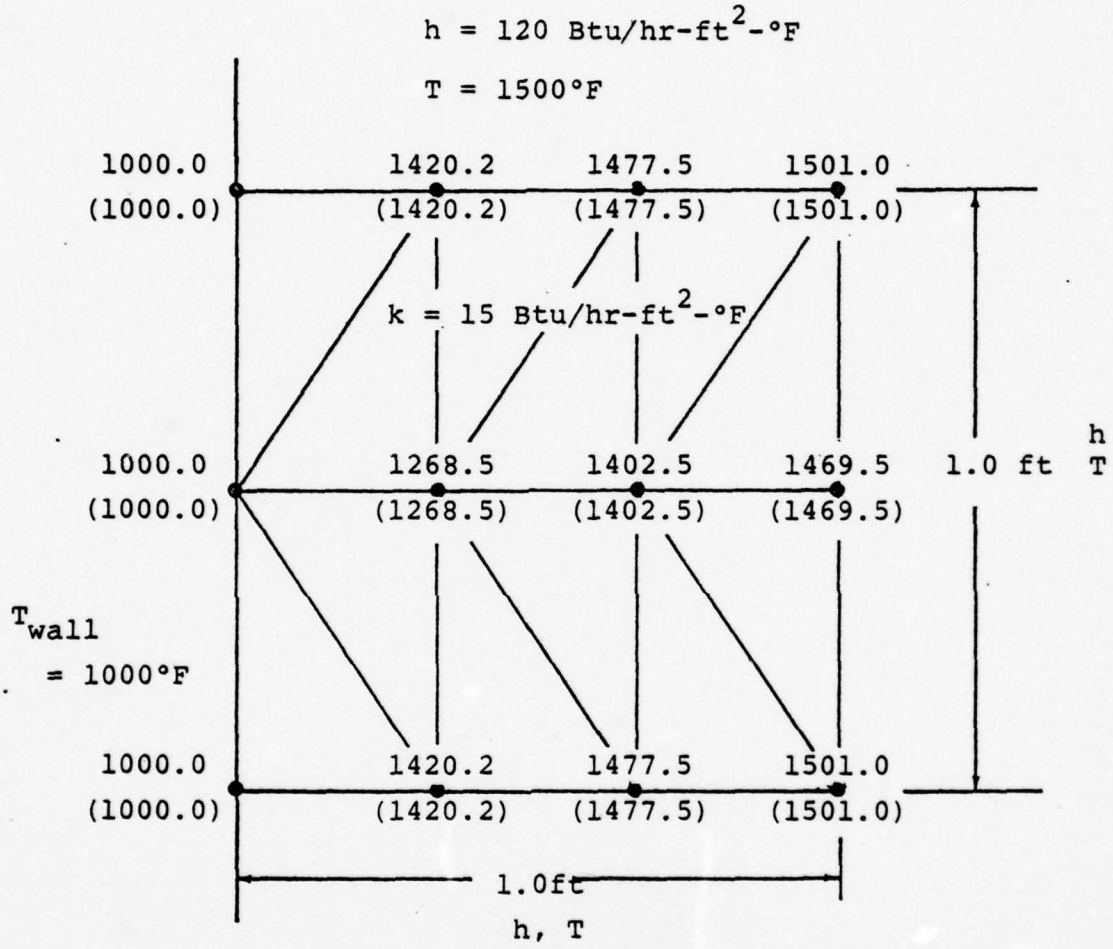

$$Q = \begin{cases} 29894.\ \text{Btu/hr} \\ (29894.\ \text{Btu/hr}) \end{cases}$$

Note: numbers in parenthesis refer to the results of reference 9

Figure 17 Statement and Results of Test Case 1

T = 100°F

h = 100. Btu/hr-ft^2-deg F

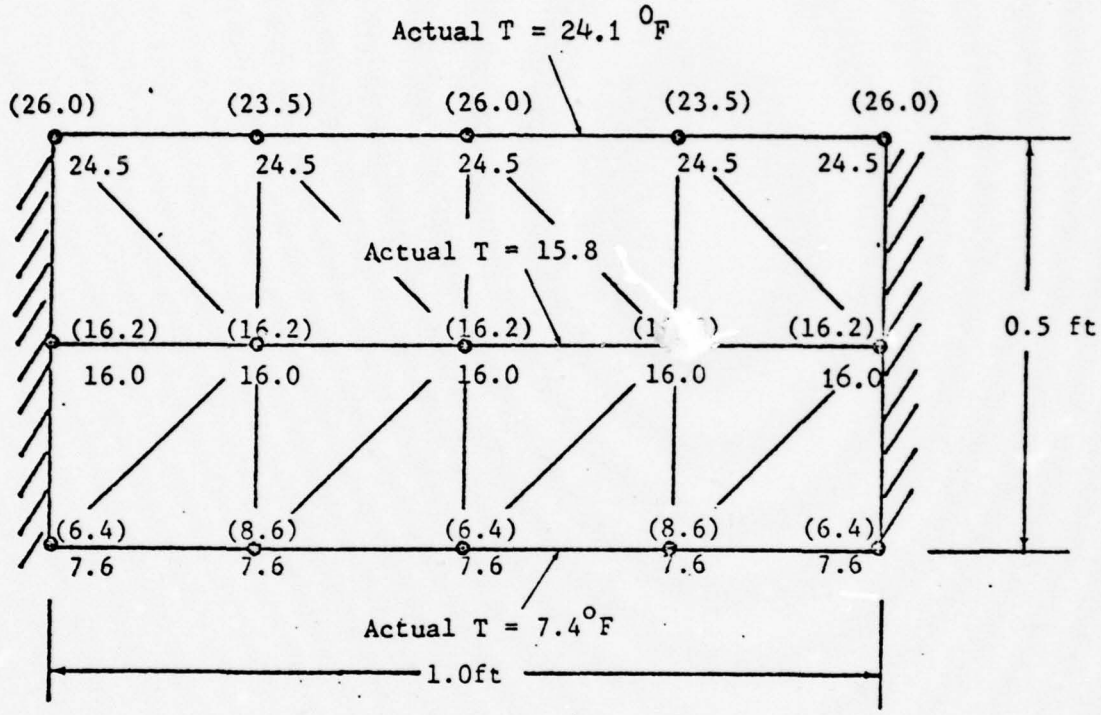

T = 0°F

h = 1000.0 Btu/hr-ft^2-deg F

Q = { 7586. Btu/hr actual
7552. Btu/hr
(7527. Btu/hr)

Note: Numbers in parentheses refer to results of Corley [6].

Figure 18. Statement and Results of Test Case 2

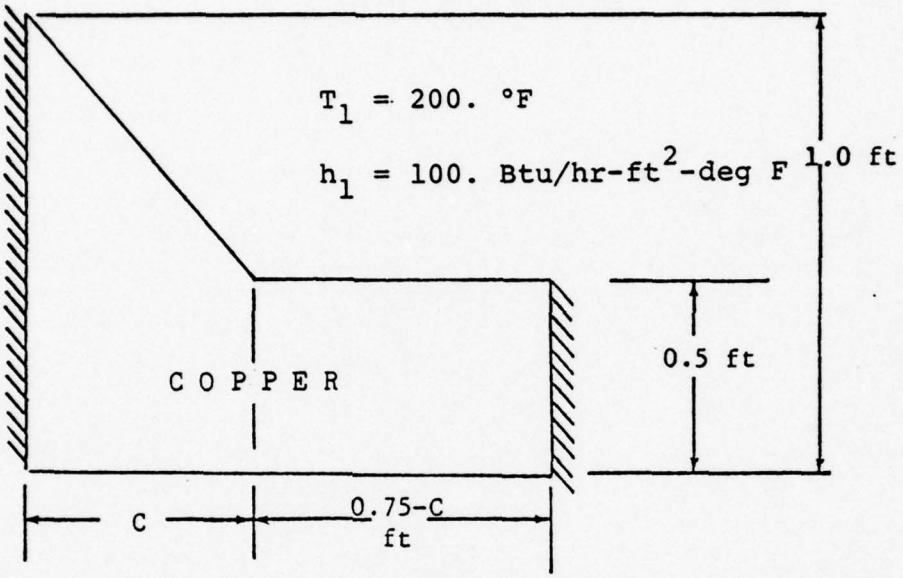

C (ft)	HEAT TRANSFER RATE (Btu/hr)		
	ONE DIMENSIONAL *)	TWO DIMENSIONAL *)	TWO DIMENSIONAL
0.25	6526.	6727.	6826.
0.05	6561.	6754.	6759.

*) Results of Corley [6]

Figure 19 Statement and Results of Test Case 3

III. NUMERICAL RESULTS AND DISCUSSION

The analysis concerns itself with the geometry of both a copper and stainless steel condenser as tabulated in Table 4, using water as the working fluid.

TABLE 4

Specification of a Typical Internally Finned Rotating Heat Pipe

Condenser length	=	9.000	inches
Minimum radius	=	0.775	inches
Wall thickness	=	0.03125	inches
Height of fin	=	0.025	inches
Cone half angle	=	1.0	degree

Results are given in Tables 5 to 18 and Figures 20 to 28. It can be seen from the data that the solution of the Finite Element Method converges. This can be seen by examining data of temperature distribution within the fins of 25, 40, and 108 linear triangular finite elements (Tables 7 to 9), for the same location (nodes 10, 15, and 28 respectively).

The heat transfer rate solution is generally affected in the same manner as the analysis of Schafer [5] when the outside convective heat transfer coefficient (h_{out}), rotational speed (ω), fin angle (2α), and thermal conductivity (k_{wall})

TABLE 5

Comparison of Theoretical Heat Transfer Rate on a Copper Finned Condenser at 1000 RPM, for h_{out} = 1000.0 Btu/hr-ft^2-deg.F

Fin half angle	No. of fins	T_{sat}	ONE DIMENSIONAL *)	ISOPARAMETRIC			TRIANGULAR		
				2 EL .)	3 EL x)	4 EL x)	25 EL	40 EL	108 EL
10.	276	100.	5720.0	10191.7	10161.4	10156.3	10220.0	10216.0	10211.0
		150.	14914.0	27125.9	27027.7	27006.8	27207.0	27195.0	27180.0
		200.	24072.0	44046.9	43878.6	43840.9	44180.0	44160.0	44134.0
30.	84	100.	5697.0	9998.8	9952.7	9907.9	9988.1	9982.0	9974.4
		150.	14815.0	26611.7	26466.3	26320.3	26532.0	26515.0	26494.0
		200.	23888.0	43210.5	42960.1	42708.8	43050.0	43023.0	42988.0
50.	40	100.		9758.7	9696.9	9626.0	9697.2	9687.2	9678.9
		150.		25965.8	25775.0	25555.0	25697.0	25669.0	25646.0
		200.		42156.4	41831.4	41459.3	41660.0	41614.0	41577.0

*) Results of Schafer [5]
x) Results of Tantrakul [4]
.) Results of Corley [6]

TABLE 6

Comparison of Theoretical Heat Transfer Rate on a Cooper Finner Condenser at 3000 RPM, for h_{out} = 1000. Btu/hr-ft^2-deg.F

Fin half angle	No. of fins	T_{sat}	ONE DIMENSIONAL *)	ISOPARAMETRIC			TRIANGULAR		
				2 EL .)	3 EL x)	4 EL x)	25 EL	40 EL	108 EL
10.	276	100.	6193.0	10273.1	10255.2	10256.9	10286.0	10283.0	10279.0
		150.	16266.0	27355.8	27308.9	27310.8	27399.0	27391.0	27380.0
		200.	26223.0	44427.2	44351.6	44353.4	4450310	44489.0	44471.0
30.	84	100.	6303.0	10095.3	10071.2	10059.6	10131.0	10126.0	10119.0
		150.	16224.0	26866.0	26795.9	26755.0	26955.0	26940.0	26922.0
		200.	26290.0	43622.0	43504.0	43431.4	43762.0	43738.0	43708.0
50.	40	100.		9870.9	9836.9	9809.6	9925.9	9917.8	9910.9
		150.		26255.7	26155.0	26065.7	26372.0	26349.0	26329.0
		200.		42623.3	42452.9	42298.0	42795.0	42757.0	42725.0

*) Results of Schafer [5]
x) Results of Tantrakul [4]
.) Results of Corley [6]

TABLE 7

Comparison of Theoretical Heat Transfer Rate on a Copper Finned Condenser at 1000 RPM, for h_{out} = 5000. Btu/hr-ft^2-deg.F

Fin half angle	No. of fins	T_{sat}	ONE DIMENSIONAL *)	ISOPARAMETRIC			TRIANGULAR		
				2 EL .)	3 EL x)	4 EL x)	25 EL	40 EL	108 EL
10.	276	100.	20983.0	43925.1	43160.3	42892.9	44412.0	44313.0	44190.0
		150.	53680.0	116132.5	113809.4	112962.4	117130.0	116840.0	116490.0
		200.	85619.0	188087.0	184090.4	182658.8	189490.0	189010.0	188420.0
30.	84	100.	18794.0	40850.6	39745.0	38564.0	39252.0	39154.0	39034.0
		150.	46893.0	108189.0	104861.7	101354.7	102260.0	102000;0	101690.0
		200.	74539.0	175334.0	169675.6	163810.7	164810.0	164390.0	163890.0
50.	40	100.		37808.3	36586.2	35173.2	34765.0	34625.0	34516.0
		150.		100094.8	96506.5	92429.3	89600.0	89227.0	88953.0
		200.		162188.9	156162.4	149403.1	143950.0	143350.0	142910.0

*) Results of Schafer [5]
.) Results of Corley [6]
x) Results of Tantrakul [4]

TABLE 8

Comparison of Theoretical Heat Transfer Rate on a Copper Finned Condenser at 3000 RPM, for h_{out} = 5000. Btu/hr-ft^2-deg.F

Fin half angle	No. of fins	T_{sat}	ONE DIMENSIONAL *)	ISOPARAMETRIC			TRIANGULAR		
				2 EL .)	3 EL x)	4 EL x)	25 EL	40 EL	108 EL
10.	276	100.	22896.0	45685.4	45368.9	45345.7	46162.0	46090.0	45994.0
		150.	59634.0	120807.7	119423.1	119244.1	122220.0	122070.0	121790.0
		200.	96156.0	195703.4	192967.8	192584.0	198180.0	197820.0	197370.0
30.	84	100.	21927.0	42327.3	41755.9	41279.3	42568.0	42465.0	42337.0
		150.	56342.0	111871.5	109985.2	108361.5	111970.0	111680.0	111340.0
		200.	90394.0	181198.5	177870.8	174935.3	181040.0	180570.0	180010.0
50.	40	100.		39287.1	38552.0	37789.8	39201.0	39056.0	38933.0
		150.		103724.0	101453.3	99075.1	102360.0	101960.0	101630.0
		200.		167950.6	163980.4	159823.7	165130.0	164490.0	163960.0

*) Results of Schafer [5]
.) Results of Corley [6]
x) Results of Tantrakul [4]

TABLE 9

Theoretical Heat Transfer Rate on a Stainless Steel Finned Condenser at 1000 RPM, for h_{out} = 1000. Btu/hr-ft^2-deg.F

Fin half angle	No. of fins	T_{sat} (^oF)	Q(Btu/hr)		
			25 EL	40 EL	108 EL
10	276	100	8948.2	8944.1	8893.9
		150	23764.0	23727.0	23607.0
		200	38557.0	38492.0	38286.0
30	84	100	8515.5	8494.4	8461.8
		150	22511.0	22445.0	22354.0
		200	36467.0	36355.0	36204.0
50	40	100	8186.3	8164.6	8141.6
		150	21574.0	21508.0	21442.0
		200	34916.0	34805.0	34693.0

TABLE 10

Theoretical Heat Transfer Rate on a Stainless Steel Finned Condenser at 3000 RPM, for h_{out} = 1000. Btu/hr-ft^2-deg.F

Fin half angle	No. of fins	T_{sat} (^oF)	Q(Btu/hr)		
			25 EL	40 EL	108 EL
10	276	100.	9096.4	9100.4	9058.1
		150.	24193.0	24200.0	24098.0
		200.	39277.0	39284.0	39123.0
30	84	100.	8818.4	8810.3	8786.0
		150.	23389.0	23376.0	23301.0
		200.	37934.0	37900.0	37781.0
50.	40	100.	8584.1	8580.7	8561.1
		150.	22720.0	22690.0	22642.0
		200.	36823.0	36768.0	36689.0

TABLE 11

Theoretical Heat Transfer Rate on a Stainless Steel Finned Condenser at 1000 RPM, for h_{out} = 5000. Btu/hr-ft^2-deg.F

Fin half angle	No. of fins	T_{sat} (^oF)	Q(Btu/hr)		
			25 EL	40 EL	108 EL
10	276	100.	26899.0	26775.0	26308.0
		150.	70520.0		68673.0
		200.	113950.0	113300.0	110780.0
30	84	100.	22742.0	22540.0	22286.0
		150.	58879.0	58288.0	57582.0
		200.	94734.0	93748.0	92581.0
50	40	100.	20426.0	20253.0	20086.0
		150.	52480.0	51978.0	51513.0
		200.	84275.0	83443.0	82676.0

TABLE 12

Theoretical Heat Transfer Rate on a Stainless Steel Finned Condenser at 3000 RPM, for h_{out} = 5000. Btu/hr-ft^2-deg.F

Fin half angle	No. of fins	T_{sat} (^oF)	Q(Btu/hr)		
			25 EL	40 EL	108 EL
10	276	100	28705.0	28701.0	28263.0
		150	75738.0	75734.0	74492.0
		200	122610.0	122620.0	120570.0
30	84	100	25604.0	25534.0	25300.0
		150	66822.0	66734.0	65951.0
		200	107830.0	107800.0	106260.0
50	40	100	23673.0	23555.0	23410.0
		150	61488.0	61127.0	60726.0
		200	99069.0	98464.0	97803.0

TABLE 13

Temperature Distribution Within the Fin at the 10^{th} Increment.
(Copper Condenser with 25 Finite Elements

NP	T(°F)	NP	T(°F)	NP	T(°F)
1	98.99	15	98.08		
2	98.79	16	97.94		
3	98.77	17	98.00		
4	98.60	18	97.99		
5	98.58	19	97.97		
6	98.53	20	97.93		
7	98.43	21	97.80		
8	98.41				
9	98.35				
10	98.23				
11	98.01				
12	98.18				
13	98.17				
14	98.14				

α = 50 deg
T_∞ = 70°F
h_{out} = 1000 Btu/hr-ft^2-deg F
RPM = 1000
T_{sat} = 100°F
Q = 9697.2 Btu/hr

TABLE 14

Temperature Distribution Within the Fin at the 10^{th} Increment
(Copper Condenser with 40 Finite Elements)

NP	T(°F)	NP	T(°F)	NP	T(°F)
1	99.01	15	98.22	29	97.90
2	98.84	16	98.04	30	97.82
3	98.83	17	97.99	31	97.79
4	98.69	18	98.17		
5	98.68	19	98.16		
6	98.64	20	98.14		
7	98.55	21	98.11		
8	98.54	22	98.06		
9	98.50	23	97.96		
10	98.45	24	97.92		
11	98.42	25	97.99		
12	98.41	26	97.98		
13	98.38	27	97.96		
14	98.32	28	97.94		

α = 50 deg T_∞ = 70°F

h_{out} = 1000 Btu/hr-ft^2-deg F RPM = 1000

T_{sat} = 100°F Q = 9687.2 Btu/hr

TABLE 15

Temperature Distribution Within the Fin at the 10^{th} Increment
(Copper Condenser with 108 Finite Elements

NP	T(°F)	NP	T(°F)	NP	T(°F)
1	99.04	24	98.39	50	97.90
2	98.91	26	98.33	51	98.05
3	98.90	28	98.20	52	97.96
4	98.79	29	98.05	58	97.85
6	98.76	30	97.99	60	97.84
7	98.68	31	97.96	61	97.97
8	98.68	32	98.27	62	97.96
10	98.63	34	98.25	63	97.95
11	98.58	36	98.20	64	97.94
13	98.56	38	98.12	65	97.92
15	98.51	39	98.02	66	97.90
16	98.49	40	97.96	67	97.90
18	98.47	41	97.94	68	97.88
19	98.45	42	98.14	69	97.82
21	98.37	44	98.04	70	97.78
22	98.41	48	97.91	71	97.76

α = 50 deg T_∞ = 70°F

h_{out} = 1000 Btu/hr-ft^2-deg F RPM = 1000

T_{sat} = 100°F Q = 9678.9 Btu/hr

TABLE 16

Temperature Distribution Within the Fin at the 10^{th} Increment
(Stainless Steel Condenser with 25 Finite Elements)

NP	T(°F)	NP	T(°F)	NP	T(°F)
1	99.79	15	95.17		
2	99.08	16	94.44		
3	99.20	17	93.94		
4	99.19	18	93.91		
5	98.24	19	93.83		
6	98.37	20	93.69		
7	97.23	21	93.11		
8	97.21				
9	97.10				
10	96.66				
11	95.48				
12	95.50				
13	95.47				
14	95.36				

α = 50 deg	T_∞ = 70°F
h_{out} = 1000 But/hr-ft^2-deg F	RPM = 1000
T_{sat} = 100°F	Q = 8186.3 Btu/hr

TABLE 17

Temperature Distribution Within the Fin at the 10^{th} Increment
(Stainless Steel Condenser with 40 Finite Elements)

NP	T(°F)	NP	T(°F)	NP	T(°F)
1	99.82	15	96.70	29	93.62
2	99.31	16	95.73	30	93.26
3	99.39	17	95.50	31	93.12
4	98.67	18	95.50		
5	98.72	19	95.48		
6	98.84	20	95.41		
7	97.97	21	95.30		
8	97.99	22	95.12		
9	98.03	23	94.62		
10	98.09	24	94.45		
11	97.25	25	93.93		
12	97.24	26	93.91		
13	97.20	27	93.85		
14	97.08	28	93.75		

α = 50 deg	T_∞ = 70°F
h_{out} = 1000 Btu/hr-ft^2-deg F	RPM = 1000
T_{sat} = 100°F	Q = 8164.6 Btu/hr

TABLE 18

Temperature Distribution Within the Fin at the 10^{th} Increment
(Stainless Steel Condenser with 108 Finite Elements)

NP	T(°F)	NP	T(°F)	NP	T(°F)
1	99.84	24	97.21	50	94.46
2	99.50	26	97.13	51	94.39
3	99.54	28	96.64	52	94.64
4	99.09	29	95.83	58	94.29
6	99.19	30	95.52	60	93.83
7	98.65	31	95.43	61	93.76
8	98.67	32	96.32	62	93.87
10	98.81	34	96.28	63	93.84
11	98.19	36	96.15	64	93.79
13	98.23	38	95.82	65	93.73
15	98.36	39	95.31	66	93.64
16	97.70	40	95.03	67	93.55
18	97.72	41	94.95	68	93.31
19	97.73	42	95.45	69	93.31
21	97.73	44	95.41	70	93.13
22	97.22	48	95.04	71	93.07

α = 50 deg	T_∞ = 70°F
h_{out} = 1000 Btu/hr-ft^2-deg F	RPM = 1000
T_{sat} = 100°F	Q = 8141.6 Btu/hr

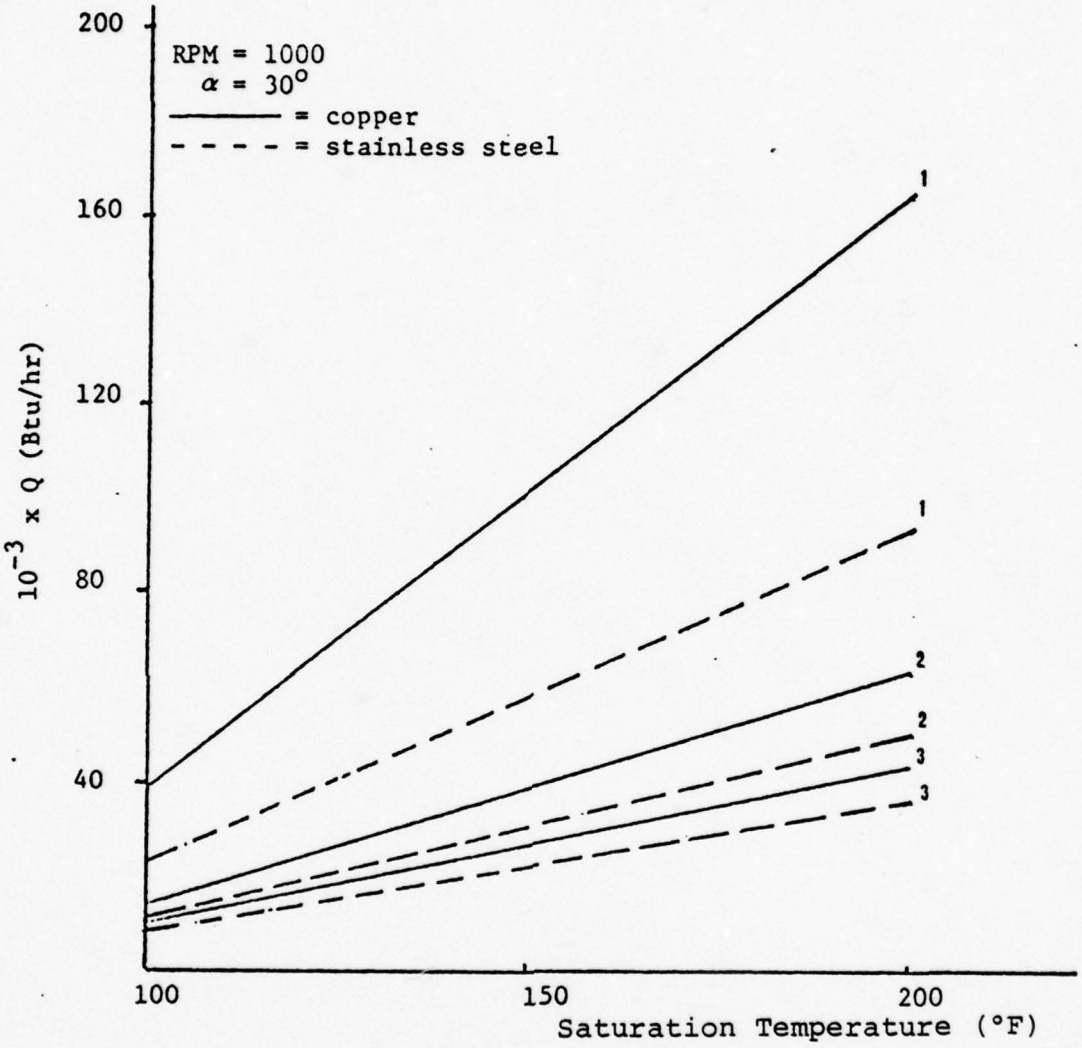

1. h_{out} = 5000 Btu/hr-ft^2-deg F
2. h_{out} = 1500 Btu/hr-ft^2-deg F
3. h_{out} = 1000 Btu/hr-ft^2-deg F

Figure 20 Heat Transfer Rate (Q) of Internally Finned Condenser at a Particular Value of h_{out}, vs. Saturation Temperature of Working Fluid

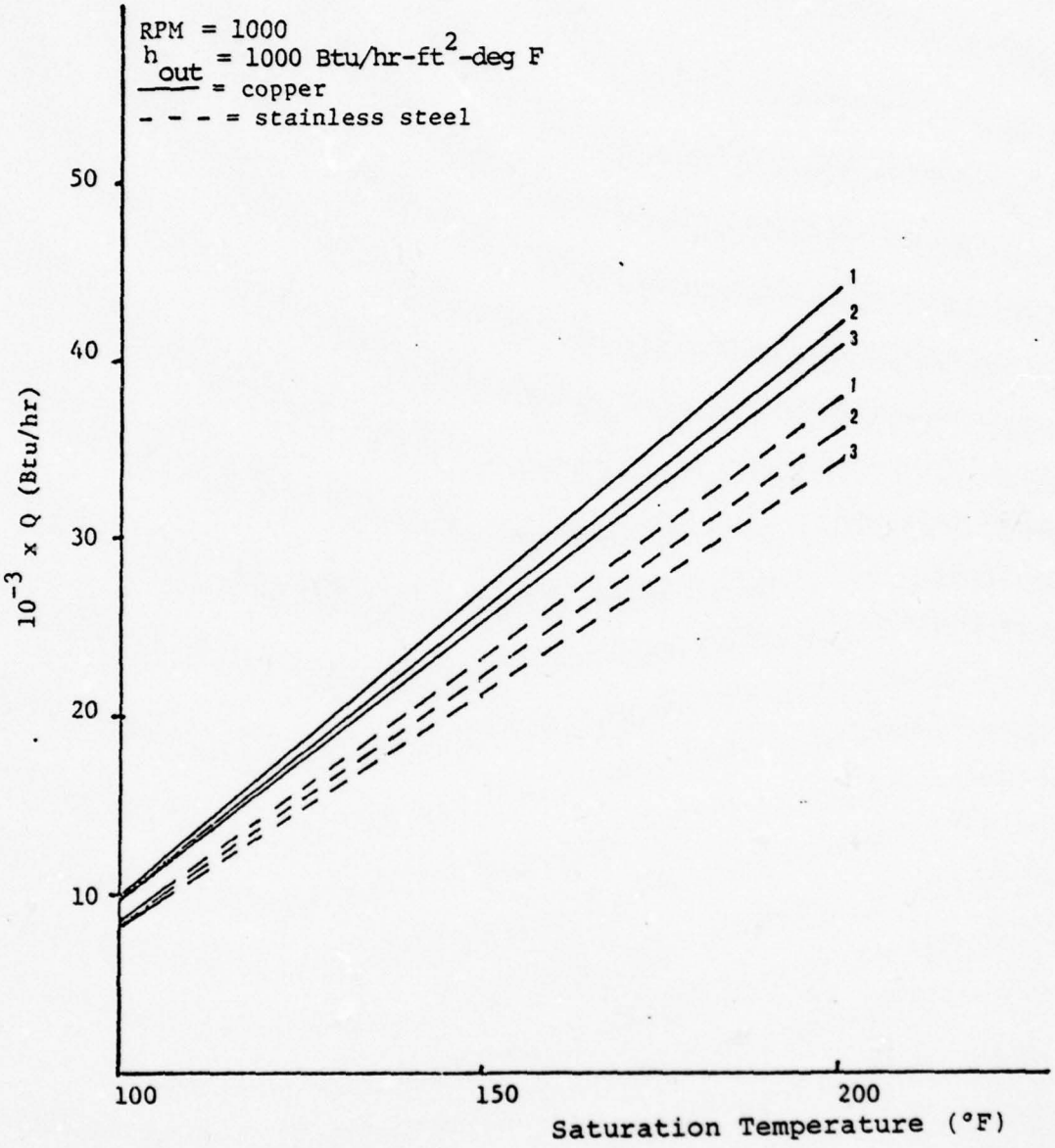

1. $\alpha = 10°$
2. $\alpha = 30°$
3. $\alpha = 50°$

Figure 21 Heat Transfer Rate (Q) of Internally Finned Condenser at a Particular Value of Fin Half Angle vs. Saturation Temperature of Working Fluid

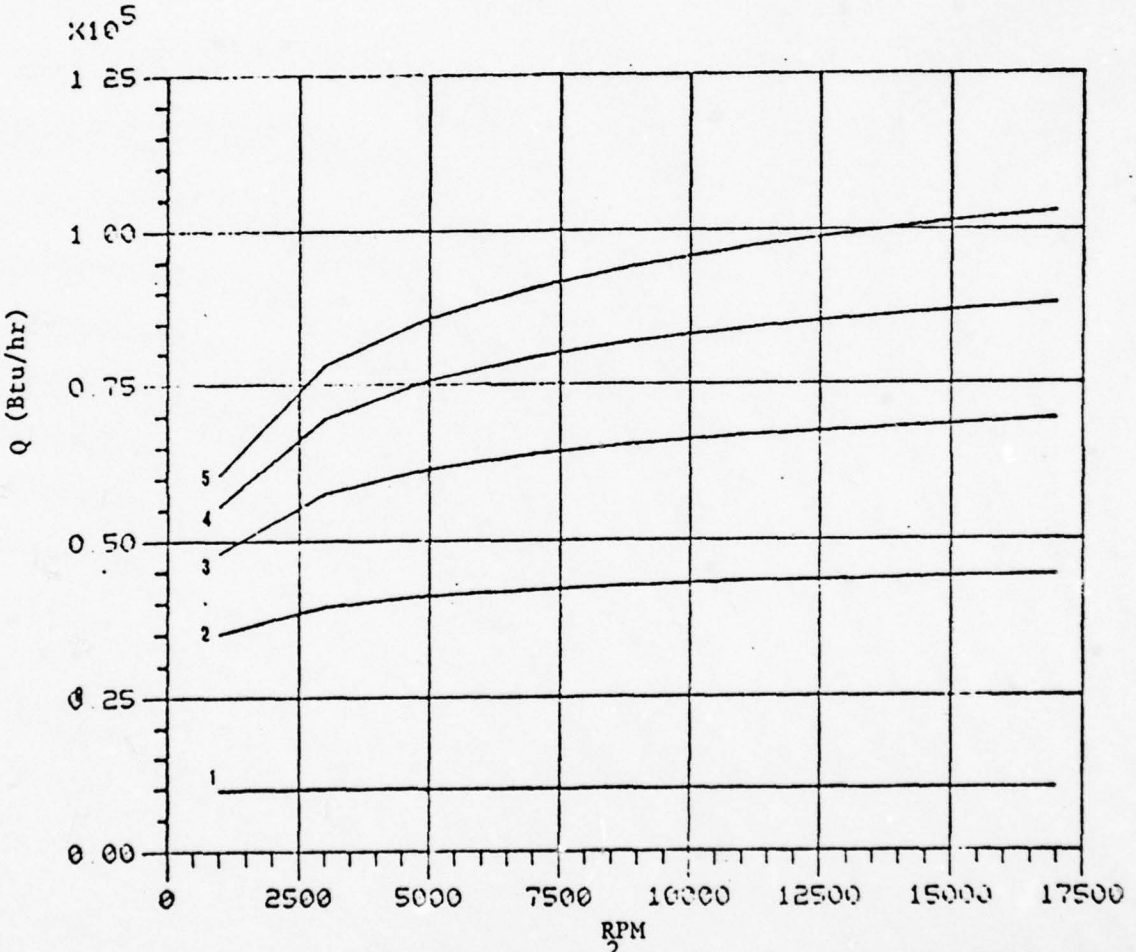

1. h_{out} = 1000. Btu/hr-ft^2-degF
2. h_{out} = 5000. Btu/hr-ft^2-degF
3. h_{out} = 9000. Btu/hr-ft^2-degF
4. h_{out} = 13000. Btu/hr-ft^2-degF
5. h_{out} = 17000. Btu/hr-ft^2-degF

Figure 22 Heat Transfer Rate (Q) of Internally Finned Copper Condenser vs. RPM

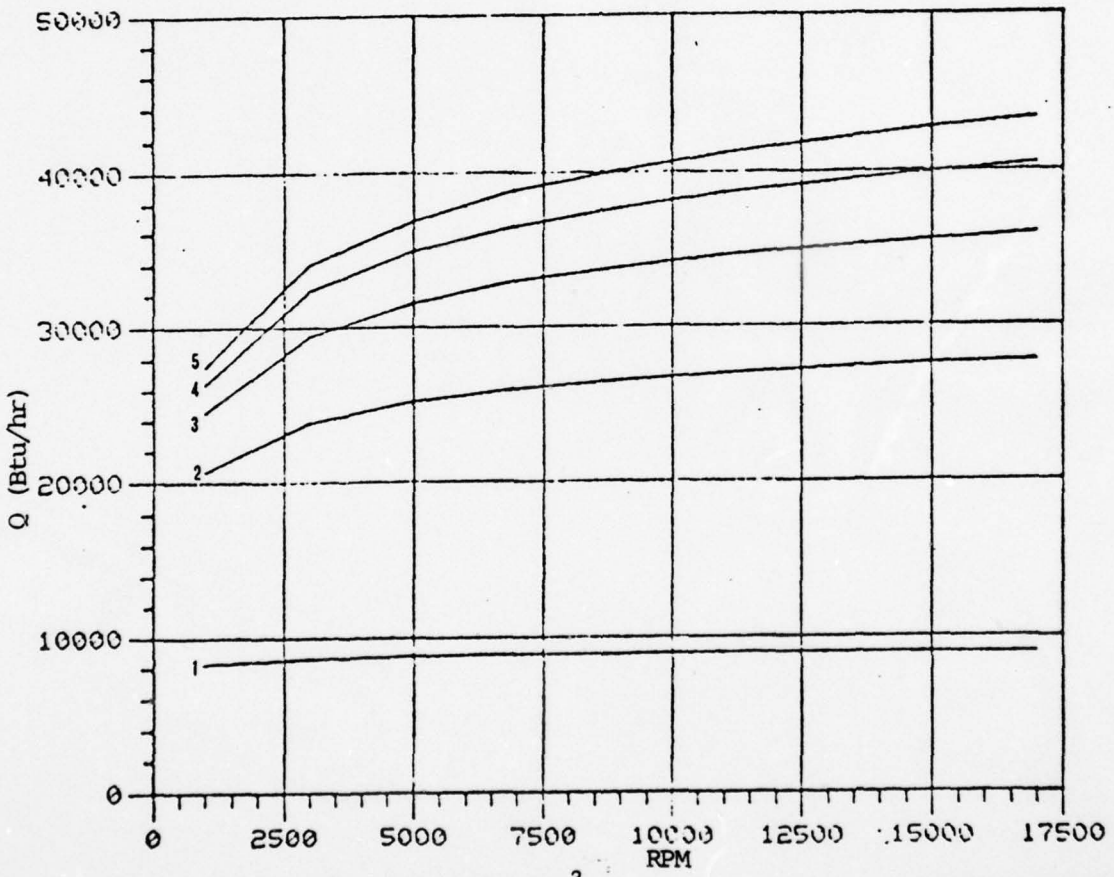

1. h_{out} = 1000. Btu/hr-ft^2-degF
2. h_{out} = 5000. Btu/hr-ft^2-degF
3. h_{out} = 9000. Btu/hr-ft^2-degF
4. h_{out} = 13000. Btu/hr-ft^2-degF
5. h_{out} = 17000. Btu/hr-ft^2-degF

Figure 23 Heat Transfer Rate (Q) of Internally Finned Stainless Steel Condenser vs. RPM

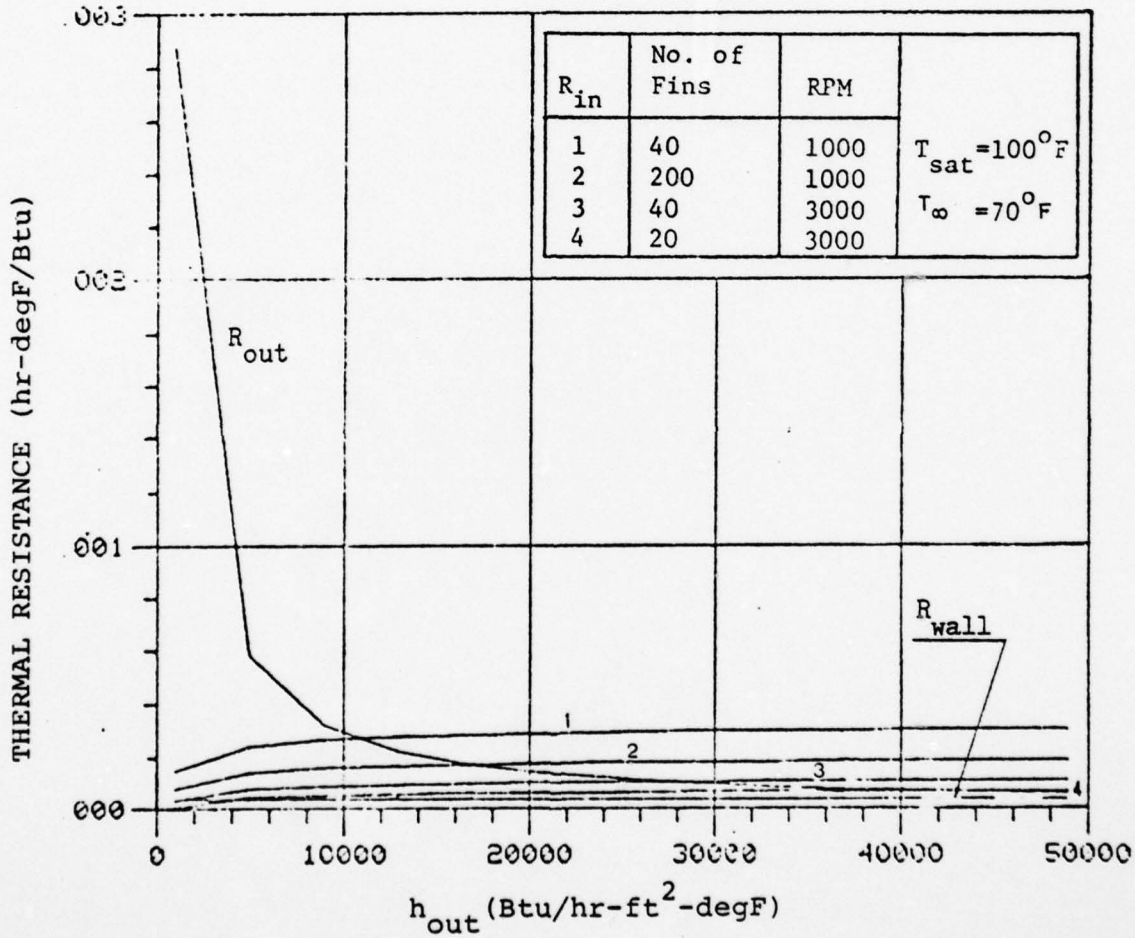

Figure 24 Thermal Resistance of Internally Finned Copper Condenser vs. h_{out}

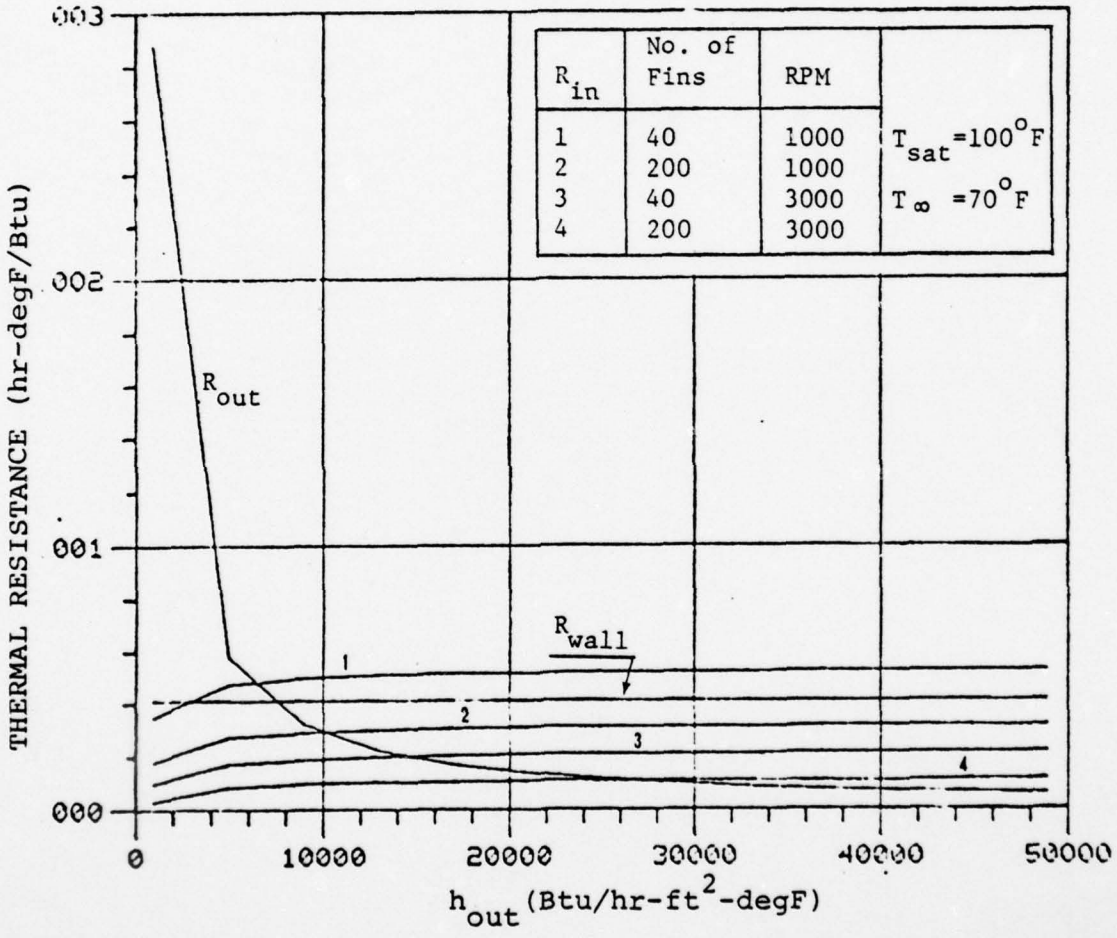

Figure 25 Thermal Resistance of Internally Finned Stainless Steel Condenser vs. h_{out}

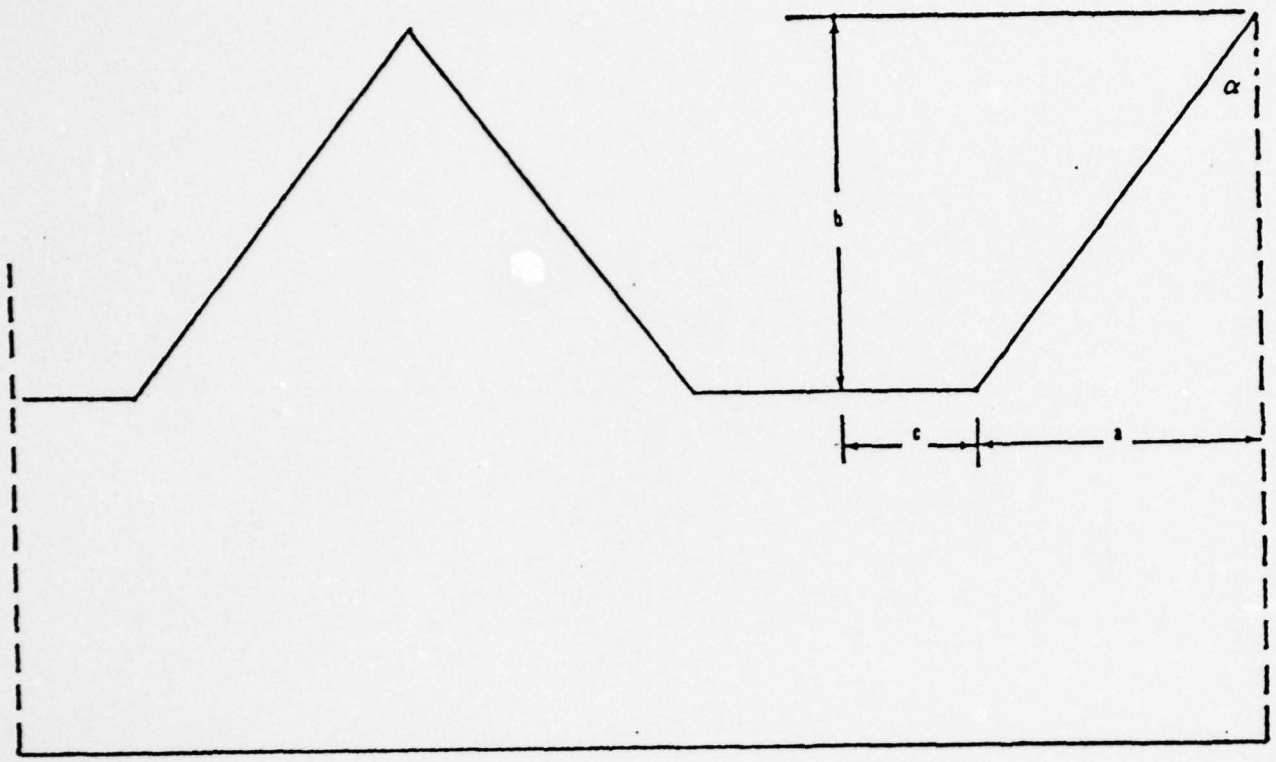

Figure 26 Fin Parameters

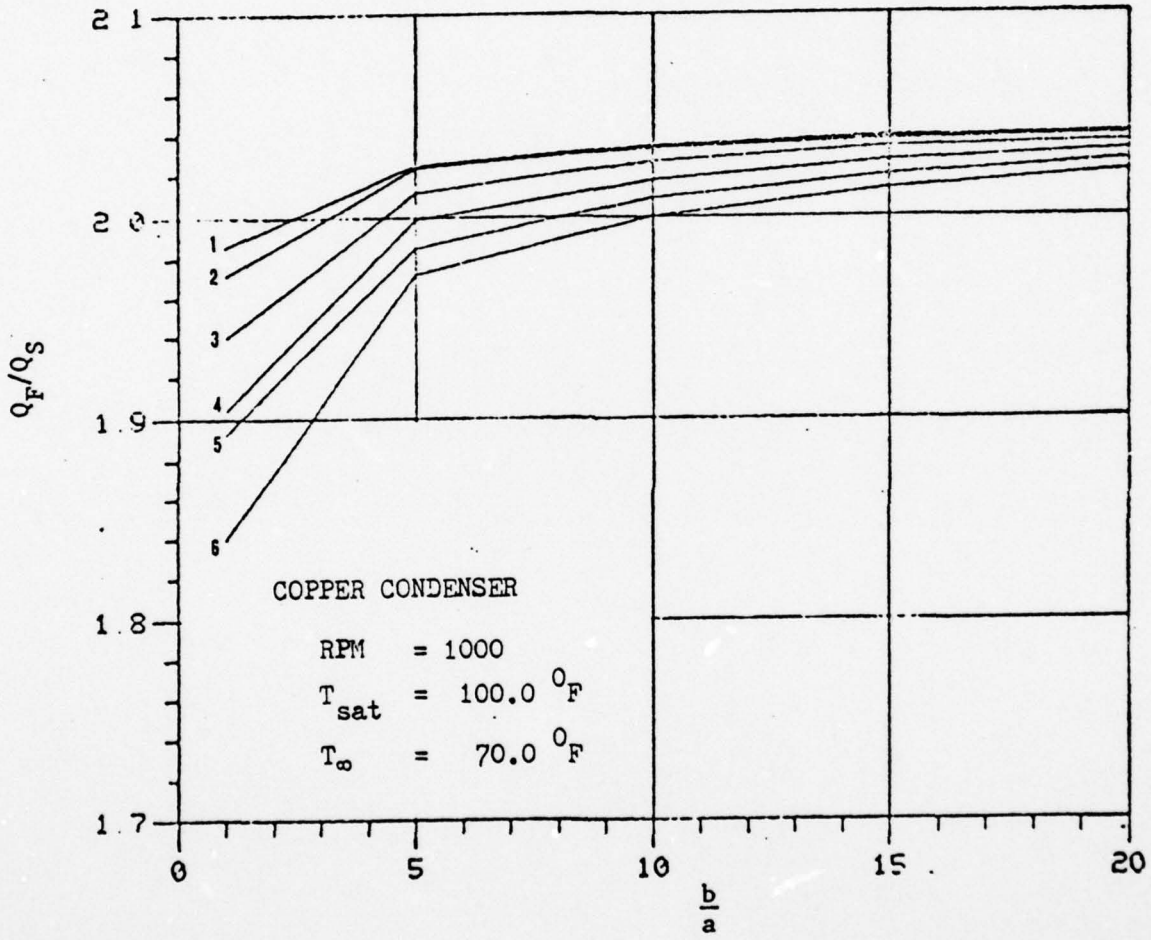

1. $\frac{c}{a} = 0.01$
2. $\frac{c}{a} = 0.1$
3. $\frac{c}{a} = 0.5$
4. $\frac{c}{a} = 1.$
5. $\frac{c}{a} = 1.5$
6. $\frac{c}{a} = 2.$

Q_F : heat transfer rate of internally finned condenser

Q_S : heat transfer rate of smooth condenser

Figure 27 Comparison of Heat Transfer Rate (Q_F/Q_S) vs. $\frac{b}{a}$ at h_{out} = 1000. Btu/hr-ft^2-degF

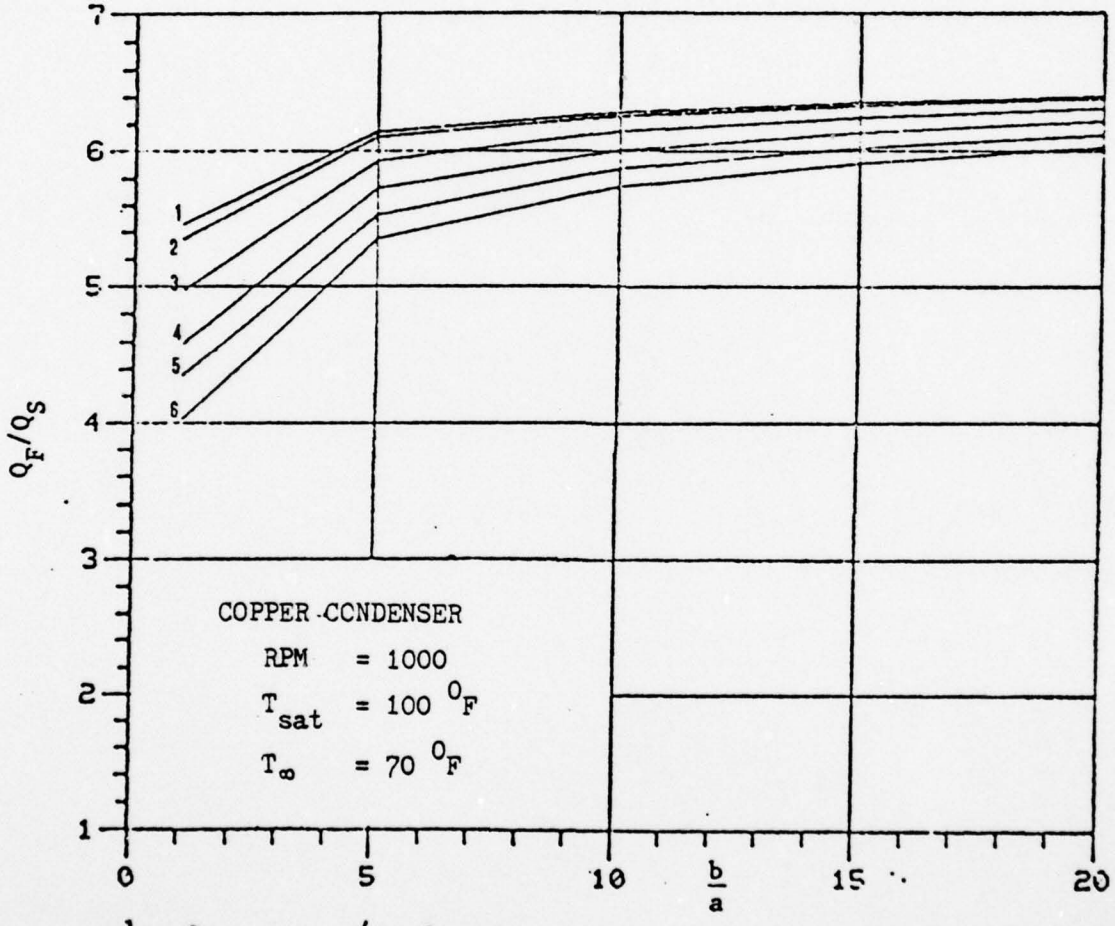

1. $\frac{c}{a}$ = 0.01
2. $\frac{c}{a}$ = 0.1
3. $\frac{c}{a}$ = 0.5
4. $\frac{c}{a}$ = 1.
5. $\frac{c}{a}$ = 1.5
6. $\frac{c}{a}$ = 2.

Q_F : heat transfer rate of internally finned condenser.

Q_S : heat transfer rate of smooth condenser.

Figure 28 Comparison of Heat Transfer Rate (Q_F/Q_S) vs. $\frac{b}{a}$ at h_{out} = 5000. Btu/hr-ft^2-degF

were varied. In Figure 20, the influence of the outside convective heat transfer coefficient, h_{out}, is shown both for copper and stainless steel. Figure 21 illustrates how the rate of heat transfer was affected when the fin half angle was varied. In addition, the heat transfer rate was found not to vary significantly with rotational speed when the heat pipe operated with low values of outside convective heat transfer coefficient, h_{out}. However, for high values of h_{out}, the effect of rotational speed cannot be ignored (see Figures 22 and 23).

The small variance of the heat transfer rate with rotational speed is due to the dominancy of the outside thermal resistance, R_{out}, such that changes in the condensate film thickness, δ, will not significantly affect the total thermal resistance as shown in Figures 24 and 25. The heat transfer rate will have a large variance when the heat pipe is operated with a high value of h_{out}.

From the results of the parametric study, as shown in Figures 27 and 28, the heat transfer rate continuously increases as the fin half angle decreases (b/a increases). Since the total number of the fins in the condenser is larger with a small half angle fin, this results in an increase in the heat transfer rate. However, the increase is only slight when the fin half angle less than 11 degrees (b/a greater than 5).

The study shows the enhancement in heat transfer is larger when operating with a high value of h_{out} or when

R_{out} is small. Therefore the design operating with a high value of h_{out}, using both internal and external fins is recommended.

IV. CONCLUSIONS

1. The Finite Element Method works and converges.
2. The designer has a choice of:
   - material
   - number of fins and fin angle
   - RPM
   - h_{out}
3. The heat transfer rate increases continuously with decreasing fin angle; however, for half angle less than 11 degrees, the increase is only slight.

V. RECOMMENDATIONS

1. Manufacture internally finned heat pipe and test.
2. Manufacture internally and externally finned heat pipe and test.

APPENDIX

COMPUTER PROGRAM LISTING

```
C  ***********************************************************
C  *                                                         *
C  *                                                         *
C  *  TWO DIMENSIONAL HEAT CONDUCTION FINITE ELEMENT ANALYSIS  *
C  *  OF ROTATING HEAT PIPE , USING TRIANGULAR ELEMENT MODEL   *
C  *  COMPILED BY MAJOR IGNATIUS S.PURNOMO IN JUNE ,1978       *
C  *                                                         *
C  *                                                         *
C  ***********************************************************
      IMPLICIT REAL*8(A-H,O-Z)
      DIMENSION Z(200),EPS(200),HZ(200),XCOF(5),COF(5),ROOTR(4),ROOTI(^
4)
     *,T(200),QB(200),DMDOT(200),UF(200),CF(200),RHOF(200),DEL(200),CW^
(2
     *00),AMTOT(200),R(200),QINC(200),TB(200),TT(200),TBM(200),TE(200)^
,T
     *IB(200),NC(200)
      DIMENSION TSS(3),FANGL(3),HINF(3),MRPM(3)
      COMMON/APOL/DOBF,DOTH,KFIN(50),KFF(50),IFF,JTC,JLC,JINT,KT
      COMMON/MAFO/A(200,50),F(200,1),H(200),TS(200),TSAT,CK,NEL,NSNP,N^
BA
     *N,ICOR(200,3)
      COMMON/PCRD/X(200),Y(200),EZERO,BVIN,THICK,TALFA,APS
      HDEN(A1,B1,ZZ)=(-1.0D0*(A1*ZZ**3/3.0D0+B1*ZZ**2/2.0D0))
C
C              ELEMENT CONNECTIVITIES
C
      READ(5,100) NEL,NSNP,NBAN
  100 FORMAT(3I5)
      WRITE(6,150) NEL,NSNP,NBAN
  150 FORMAT(/2X,'NO.OF.ELEMENTS=',I5,10X,'NO.OF SYSTEM N.P.=',I5,10X,^
'N
     *O.OF BANDED=',I5)
```

```
      READ(5,200) (IEL,(ICOR(IEL,I),I=1,3),IEL=1,NEL)
  200 FORMAT(4I5)
      WRITE(6,250)
  250 FORMAT(/2X,'ELEMENT',10X,'NP1',14X,'NP2',15X,'NP3')
      WRITE(6,251)(IEL,(ICOR(IEL,I),I=1,3),IEL=1,NEL)
  251 FORMAT(I5,12X,I5,12X,I5,12X,I5)
C
C             THE CONDENSER GEOMETRY
C             CL IS THE CONDENSER LENGTH
C             CANGL IS THE CONE HALF ANGLE
C             RBASE IS THE CONDENSER RADIUS AT THE BASE
C             THICK IS THE WALL THICKNESS OF THE CONDENSER
C
      READ(5,300) CL,CANGL,RBASE,R2,THICK,BFIN
  300 FORMAT(6G10.5)
      CL=CL/12.0D0
      R2=R2/12.0D0
      RBASE=RBASE/12.0D0
      BFIN=BFIN/12.0D0
C
C             NDIV IS THE NUMBER OF INCREMENT
C             NEST IS THE ELEMENT NUMBER AT THE END OF THE TROUGH
C             NEFB IS THE ELEMENT NUMBER AT THE BASE OF THE FIN
C             NBOTI IS THE FIRST ELEMENT AT THE BOTTOM SIDE
C             NBOTF IS THE LAST ELEMENT AT THE BOTTOM SIDE
C
      READ(5,400) NDIV,NEST,NEFB,NBOTI,NBOTF
  400 FORMAT(5I5)
      DIV=DFLOAT(NDIV)
      PI=3.1415926535897D0
      PHI=2.0D0*CANGL*PI/360.0D0
      SPHI=DSIN(PHI)
      CPHI=DCOS(PHI)
      TPHI=DTAN(PHI)
```

```
      DELX=CL/DIV
      CBASE=2.0D0*PI*RBASE
      REXIT=RBASE+CL*TPHI
      CEXIT=2.0D0*PI*REXIT
      THICK=THICK/12.0D0
      WRITE(6,450)CL,CANGL,R2,THICK,RBASE,BVIN
  450 FORMAT(' ',//5X,'CONDENSER^S LENGTH=',E12.5,30X,'HALF CONE ANGLE^
='
     *,E12 5,/,5X,'R2=',E12.5,45X,'THICK=',E12.5,/,5X,'R-BASE=',E12.5,^
41
     *X,'B-FIN=',E12 5)
C
C             DATA FOR RUNNING
C
      READ(5,500) (MRPM(I),I=1,3)
  500 FORMAT(3I5)
      READ(5,600) (TSS(I),I=1,3)
  600 FORMAT(3G10 5)
      READ(5,700) TINF
  700 FORMAT(G10.5)
      READ(5,800) (HINF(I),I=1,3)
  800 FORMAT(3G10.5)
C
C             THE CONVERGENCE CRITERIAN
C
      READ(5,900) CRIT
  900 FORMAT(G10 9)
C
C             INTERNALLY FIN GEOMETRY
C
      READ(5,1000) (FANGL(I),I=1,3)
 1000 FORMAT(3G10.5)
      READ(5,1100) IFF
 1100 FORMAT(I5)
```

```
      READ(5,1200) (KFIN(I),KFF(I),I=1,IFF)
 1200 FORMAT(16I5)
      READ(5,1300)DOBF,DOTH,JTC,JLC,JINT,KT
 1300 FORMAT(2G10.5,4I5)
      NHB=NEFB/2
      NTM=NBOTI+(NBOTF-NBOTI)/2
      NEF=NBOTF+1
      WRITE(6,1350) ICOR(NBOTI,2),ICOR(NEFB,1),ICOR(NTM,2),ICOR(NEST,1^
),
     *ICOR(NBOTF,1)
 1350 FORMAT(///5X,'TIB=',I5,10X,'TT=',I5,/,5X,'TBM=',I5,10X,'TE=',I5,^
/,
     *6X,'TB=',I5)
      DO 1400 KIA=1,3
      ALFA=FANGL(KIA)*2.0D0*PI/360.0D0
      SALFA=DSIN(ALFA)
      CALFA=DCOS(ALFA)
      TALFA=DTAN(ALFA)
      EZERO=2.0D0*BVIN*TALFA
      EPSO=EZERO
      NFIN=CBASE/(EZERO+EPSO)
      EPSEX=(CEXIT-(NFIN*EZERO))/NFIN
      BETA=(EPSEX-EPSO)/DIV
      ZZERO=BVIN/CALFA
      ZA=0.0D0
C
C             BOUNDARY CONDITIONS AND TEMPERATURE'S ESTIMATE
C             ALONG THE FIN BOUNDARY
C
      DO 1450 NTINF=NBOTI,NBOTF
 1450 TS(NTINF)=TINF
      DO 1500 NNT=NBF,NEL
      TS(NNT)=0.0D0
 1500 H(NNT)=0.0D0
```

AD-A059 694 NAVAL POSTGRADUATE SCHOOL MONTEREY CALIF F/G 13/1
THE ENHANCEMENT OF HEAT TRANSFER IN A ROTATING HEAT PIPE.(U)
JUN 78 I S PURNOMO

UNCLASSIFIED NL

2 OF 2
ADA
059694

END
DATE
FILMED
12-78
DDC

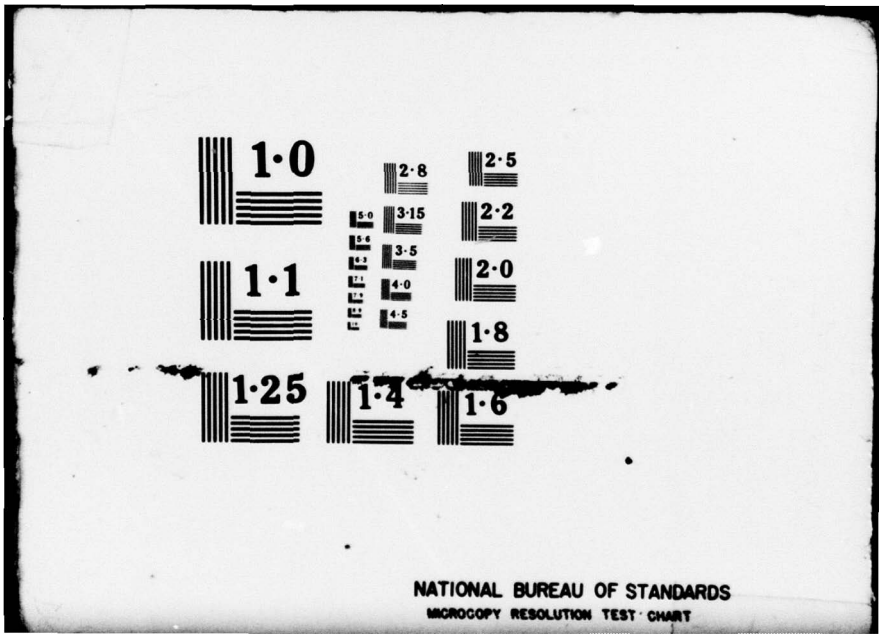
1·0
1·1
1·25
2·8
3·15
3·5
4·0
4·5
1·4
2·5
2·2
2·0
1·8
1·6
NATIONAL BUREAU OF STANDARDS
MICROCOPY RESOLUTION TEST CHART

```
      DO 1600 IGT=1,NEST
      IE=ICOR(IGT,2)
 1600 READ(5,1700) T(IE)
      IG=ICOR(NEST,1)
      READ(5,1700) T(IG)
 1700 FORMAT(G10.5)
      DO 1400 KIB=1,3
      NRPM=MRPM(KIB)
      OMEGA=NRPM*2.0D0*PI*60.0D0
      DO 1400 KIC=1,3
      DO 1300 KL=NBOTI,NBOTF
 1300 H(KL)=HINF(KIC)
      HIFN=HINF(KIC)
      DO 1400 KID=1,3
      TSAT=TSS(KID)
      DO 1900 NSAT=1,NEST
 1900 TS(NSAT)=TSAT
      TSOLID=(TSAT+TINF)/2.0D0
      DEL(1)=0.00006752D0
      QT=0.0D0
      QTOT=0.0D0
      DMTOT=0.0D0
      NK=NDIV+1
      DO 2000 NI=1,NK
      R(NI)=R2+NI*DELX*SPHI
      EPS(NI)=EPS0+NI*BETA
      APS=EPS(NI)
C
C             NODAL POINTS COORDINATE
C
      CALL COORD
      Z(1)=ZA
      DO 2100 IZEL=1,NEFB
      NA=ICOR(IZEL,1)
```

```
      NB=ICOR(IZEL,2)
      XE=X(NA)-X(NB)
      YE=Y(NA)-Y(NB)
      ELZ=DSQRT(XE**2+YE**2)
 2100 Z(IZEL+1)=Z(IZEL)+ELZ
      XZB=X(ICOR(NHB,1))-X(ICOR(1,2))
      YZB=Y(ICOR(NHB,1))-Y(ICOR(1,2))
      ZB=DSQRT(XZB**2+YZB**2)
      ZC=ZZERO
    1 IM=1
C
C           PARABOLIC TEMPERATURE DISTRIBUTION ALONG THE FIN
C           BOUNDARY,USING LAGRANGE INTERPOLATION
C
    2 TP1=T(ICOR(1,2))
      TP2=T(ICOR(NHB,1))
      TP3=T(ICOR(NEFB,1))
      AP1=TP1/(ZB*ZC)
      AP2=TP2/(ZB*(ZB-ZC))
      AP3=TP3/(ZC*(ZC-ZB))
      BP1=-(ZB+ZC)*AP1
      BP2=-ZC*AP2
      BP3=-ZB*AP3
      A1=AP1+AP2+AP3
      B1=BP1+BP2+BP3
      TC=0.0D0
      DO 2200 NY=1,NEST
 2200 TC=TC+T(ICOR(NY,2))
      AY=DFLOAT(NY+1)
      TF=(TC+T(ICOR(NY,1))+AY*TS(NY))/(2.0D0*AY)
C
C           SOLID-FLUID PROPERTIES
C
      HFG=1097.2D0-0.601875D0*TS(1)
```

```
      RHOF(NI)=62.774D0-0.00255698D0*TF-0.000053572D0*TF**2
      CF(NI)=0.3034D0+0.000738927D0*TF-0.00000147321D0*TF**2
      UF(NI)=0.001397D0-0.000014669D0*TF+0.000000631253D0*TF**2-0.000^
00
     *000000976569D0*TF**3
      UF(NI)=3600*UF(NI)
      CW(NI)=231.7772D0-0.02222D0*TSOLID
      CK=CW(NI)
      CONST=RHOF(NI)**2*OMEGA**2*HFG*CPHI*CALFA*R(NI)
C
C             AVERAGE ELEMENT CONVECTIVE COEFFICIENT ALONG THE
C             FIN BOUNDARY
C
      ZSTAR=ZZERO-DEL(NI)/CALFA
      AZZ=DEL(NI)/SALFA
      ZZ=ZSTAR
      AZS=DABS(4*CF(NI)*UF(NI)*HDEN(A1,B1,ZZ)/CONST)**0.25D0
      HAC=0.0D0
      DO 2300 IEL=1,NEFB
      AZ=Z(IEL)
      BZ=Z(IEL+1)
      IF(ZSTAR.LE.BZ) GO TO 2400
      GO TO 2500
 2400 IF(HAC.NE.0.0D0) GO TO 2600
      BZ=ZSTAR
 2500 IF(IEL.NE.1) GO TO 2700
      AK=(BZ-AZ)/5.0D0
      ZZ=AK
      GO TO 2800
 2700 AK=(BZ-AZ)/4.0D0
      ZZ=AZ
 2800 ZEL=4*AK
      DO 2900 NH=1,5
      HZ(NH)=DABS(CF(NI)**3*CONST/(4*UF(NI)*HDEN(A1,B1,ZZ)))**0.25D0
```

```
 2900 ZZ=ZZ+AK
      CONH=AK*(HZ(1)+4*HZ(2)+2*HZ(3)+4*HZ(4)+HZ(5))/(3*ZEL)
      IF(ZSTAR.EQ.BZ) GO TO 3000
      H(IEL)=CONH
      GO TO 2300
 3000 AZ=ZSTAR
      HAZ=CONH*(AZ-Z(IEL))
      DELA=AZS
 3100 BZ=Z(IEL+1)
      DELB=(BZ-ZSTAR)*AZZ/(ZZERO-ZSTAR)
      DELZ=(DELA+DELB)/2.0D0
      HAC=(BZ-AZ)*CF(NI)/DELZ
      H(IEL)=(HAZ+HAC)/(BZ-Z(IEL))
      GO TO 2300
 2600 AZ=Z(IEL)
      DELA=DELB
      HAZ=0.0D0
      GO TO 3100
 2300 CONTINUE
      NETI=NEFB+1
      DO 3200 IEL=NETI,NEST
 3200 H(IEL)=CF(NI)/DEL(NI)
C
C             ENTRY INTO THE FINITE ELEMENT SOLUTION
C
      CALL FORMAF
      CALL BANDEC(NSNP,NBAN,1)
C
C             THE TEMPERATURE DISTRIBUTION
C
      DO 3300 NT=1,NSNP
 3300 T(NT)=F(NT,1)
      TIB(NI)=T(ICOR(NBOTI,2))
      TT(NI)=T(ICOR(NEFB,1))
```

```
      TBM(NI)=T(ICOR(NTM,2))
      TE(NI)=T(ICOR(NEST,1))
      TE(NI)=T(ICOR(NBOTF,1))
      TTS=0.0D0
      DO 3400 NS=1,NSNP
 3400 TTS=TTS+T(NS)
      PN=DFLOAT(NS)
      TSOLID=TTS/PN
C
C             Q AT THE BOTTOM SIDE
C
      QBI=0.0D0
      DO 3500 IBEL=NBOTI,NBOTF
      NKA=ICOR(IBEL,1)
      NKB=ICOR(IBEL,2)
      XB=X(NKA)-X(NKB)
      YB=Y(NKA)-Y(NKB)
      ELB=DSQRT(XB**2+YB**2)
 3500 QBI=QBI+(T(NKA)+T(NKB)-2*TS(IBEL))*ELB*H(IBEL)/2.0D0
      QB(NI)=QBI*DELX
C
C             ITERATION UNTIL CONVERGENCE CRITERIA IS MET
C
      IF(IM.EQ.1) GO TO 3600
      QJ=QBI
      GO TO 3700
 3600 QI=QBI
      IM=2
      GO TO 2
 3700 AQ=DABS(QJ-QI)/QJ
      IF(AQ.LE.CRIT) GO TO 3800
      QI=QJ
      GO TO 2
 3800 DMDOT(NI)=2*QBI*DELX/HFG
```

```
      DMTOT=DMTOT+DMDOT(NI)
      C1=RHOF(NI)**2*OMEGA**2*R(NI)/(3*UF(NI))
      XCOF(1)=-DMTOT
      XCOF(2)=0.0D0
      XCOF(3)=0.0D0
      XCOF(4)=C1*EPS(NI)
      XCOF(5)=C1*TALFA
      M=4
      CALL DPOLRT(XCOF,COF,M,ROOTR,ROOTI,IER)
      IF(ROOTR(1).LT.0.005D0.AND.ROOTR(1).GT.0.0D0) GO TO 3900
      IF(ROOTR(2).LT.0.005D0.AND.ROOTR(2).GT.0.0D0) GO TO 4000
      IF(ROOTR(3).LT.0.005D0.AND.ROOTR(3).GT.0.0D0) GO TO 4100
      IF(ROOTR(4).LT.0.005D0.AND.ROOTR(4).GT.0.0D0) GO TO 4200
      WRITE(6,4300)
 4300 FORMAT(//10X,'CRASH,CRASH,CRASH')
      WRITE(6,4350) (ROOTR(I),I=1,4)
 4350 FORMAT(//5X,4(E12.7,3X))
      GO TO 6100
C
C            THE CONDENSATE THICKNESS
C
 3900 DEL(NI+1)=ROOTR(1)
      GO TO 4400
 4000 DEL(NI+1)=ROOTR(2)
      GO TO 4400
 4100 DEL(NI+1)=ROOTR(3)
      GO TO 4400
 4200 DEL(NI+1)=ROOTR(4)
 4400 QEL=0.0D0
      IF(NI.NE.10) GO TO 4500
      WRITE(6,4600)
 4600 FORMAT('1',//5X,'NP',6X,'X',12X,'Y',12X,'T')
      DO 4700 NP=1,NSNP
 4700 WRITE(6,4800) NP,X(NP),Y(NP),T(NP)
```

```
 4800 FORMAT(/2X,I3,3X,3(F10.6,3X))
      WRITE(6,4900)
 4900 FORMAT(//2X,'EL',8X,'H',11X,'EL-LENGTH',15X,'Q-EL')
      DO 5000 KKL=1,NBOTF
      NKX=ICOR(KKL,1)
      NKY=ICOR(KKL,2)
      XP=X(NKX)-X(NKY)
      YP=Y(NKX)-Y(NKY)
      EXY=DSQRT(XP**2+YP**2)
      QEP=DABS((T(NKX)+T(NKY)-2*TS(KKL))*EXY*H(KKL)/2.0D0)
      QEP=QEP*DELX
 5000 WRITE(6,5100) KKL,H(KKL),EXY,QEP
 5100 FORMAT(/2X,I2,3X,E12.5,3X,E12.5,10X,E12.5)
      WRITE(6,5200) CRIT
 5200 FORMAT(/2X,'CONVERGENCE CRITERIAN=',E15.8)
C
C             Q FROM THE TOP SIDE
C
 4500 DO 5300 IQEL=1,NEST
      KA=ICOR(IQEL,1)
      KB=ICOR(IQEL,2)
      XQEL=X(KA)-X(KB)
      YQEL=Y(KB)-Y(KA)
      ELM=DSQRT(XQEL**2+YQEL**2)
      QEL=QEL+(2*TS(IQEL)-T(KA)-T(KB))*ELM*H(IQEL)/2.0D0
 5300 CONTINUE
      QINC(NI)=QEL*DELX
      AMTOT(NI)=DMTOT
      QET=QEL*DELX*NFIN*2
      QT=QT+QET
      QA=QBI*DELX*NFIN*2
      QTOT=QTOT+QA
 2000 CONTINUE
      WRITE(6,5400) HFG,NFIN,H(NBOTF),TSAT,NRPM,QTOT,QT,FANGL(KIA)
```

```
 5400 FORMAT(' ',//,5X,'HFG=',E12.5,/,5X,'NUMBER OF FIN=',I5,/,5X,'H-O^
UT
     *=',E12.5,/,5X,'TSAT=',E12.5,/,5X,'RPM=',I5,/,5X,'Q-BOT=',E12.5,/^
,5
     *X,'Q-TOP=',E12.5,/,5X,'HALF-ANGLE=',F8.3)
      WRITE(6,5500)
 5500 FORMAT('0',6X,'J',4X,'FILM THICKNESS',6X,'Q-INCREM',6X,'MASS-TOT^
',
     17X,'TIB',3X,'TT',10X,'TE',3X,'TB')
      DO 5600 NR=1,NDIV
 5600 WRITE(6,555) NR,DEL(NR),QB(NR),AMTOT(NR),TIB(NR),TT(NR),TE(NR),T^
B(
     *NR)
 555  FORMAT (' ',4X,I4,4X,F12.10,4X,F10.4,6X,F9.5,6X,F5.1,6X,F5.1,6X,^
F5
     1.1,6X,F5.1)
      WRITE(6,5800)
 5800 FORMAT('0',6X,'J',6X,'K-WALL',4X,'K-FILM',3X,'DENSITY',4X,'VISC-^
FI
     *ILM',6X,'EPSILON',5X,'RADIUS',5X,'TBM',5X,'Q-BOT')
      DO 5900 NG=1,NDIV,2
 5900 WRITE(6,777) NG,CW(NG),CF(NG),RHOF(NG),UF(NG),EPS(NG),R(NG),TBM(^
NG
     *),QINC(NG)
 777  FORMAT (' ',4X,I4,4X,F7.3,4X,F6.4,4X,F6.3,4X,F9.7,4X,F9.7,4X,F7.^
5,
     15X,F5.1,1X,1P1D12.3)
 1400 CONTINUE
 6100 STOP
      END
      SUBROUTINE COORD
      IMPLICIT REAL*8(A-H,O-Z)
      COMMON/PCRD/X(200),Y(200),EZERO,BVIN,THICK,TALFA,APS
      COMMON/APOL/DOBF,DOTH,KFIN(50),KFF(50),IFF,JTC,JLC,JINT,KT
```

```
      DELH=BVIN/DOBF
      X(1)=0.0D0
      Y(1)=THICK+BVIN
      N=1
      DO 321 I=1,IFF
      ICA=KFIN(I)
      ICB=KFF(I)
      CBA=DFLOAT(ICB-ICA)
      AN=0.0D0
      DO 322 II=ICA,ICB
      X(II)=X(1)+N*AN*DELH*TALFA/CBA
      Y(II)=Y(1)-N*DELH
  322 AN=AN+1.0D0
  321 N=N+1
      AN=0.0D0
      ICD=ICB-ICA+1
      DO 323 J=JTC,JLC,JINT
      X(J)=X(1)
      Y(J)=(1.0D0-AN/DOTH)*THICK
      DO 324 JJ=1,ICD
      X(J+JJ)=X(J)+JJ*EZERO/(2*(CBA+1.0D0))
  324 Y(J+JJ)=Y(J)
      DO 325 K=1,KT
      X(J+JJ+K)=X(J+JJ)+K*APS/(2.0D0*KT)
  325 Y(J+JJ+K)=Y(J)
  323 AN=AN+1.0D0
      RETURN
      END
      SUBROUTINE FORMAF
      IMPLICIT REAL*8(A-H,O-Z)
      DIMENSION B(3),C(3),EA(3,3)
      COMMON/PCRD/X(200),Y(200),EZERO,BVIN,THICK,TALFA,APS
      COMMON/MAFO/A(200,50),F(200,1),H(200),TS(200),TSAT,CK,NEL,NSNP,N^
BA
```

```
     *N,ICOR(200,3)
      DO 101 N=1,NSNP
      F(N,1)=0.0D0
      DO 102 MA=1,NBAN
102   A(N,MA)=0.0D0
101   CONTINUE
      DO 103 IEL=1,NEL
      IA=ICOR(IEL,1)
      IB=ICOR(IEL,2)
      IC=ICOR(IEL,3)
      B(1)=Y(IB)-Y(IC)
      B(2)=Y(IC)-Y(IA)
      B(3)=Y(IA)-Y(IB)
      C(1)=X(IC)-X(IB)
      C(2)=X(IA)-X(IC)
      C(3)=X(IB)-X(IA)
      EL=DSQRT(C(3)**2+B(3)**2)
      AS=DABS((B(1)*C(2)-B(2)*C(1))/2.0D0)
      HC=H(IEL)/CK
      DO 104 J=1,3
      JJ=ICOR(IEL,J)
      DO 105 K=1,3
      KK=ICOR(IEL,K)
      EA(J,K)=(B(J)*B(K)+C(J)*C(K))/(4*AS)
      IF(HC EQ 0.0D0) GO TO 106
      HEL=HC*EL/6.0D0
      IF(J.EQ.3) GO TO 106
      IF(K.EQ.3) GO TO 106
      IF(J.EQ.K) GO TO 107
      EA(J,K)=EA(J,K)+HEL
      GO TO 106
107   EA(J,K)=EA(J,K)+2*HEL
106   IF(KK.LT.JJ) GO TO 105
      NW=KK-JJ+1
```

```
      A(JJ,NU)=A(JJ,NU)+EA(J,K)
  105 CONTINUE
  104 CONTINUE
      FE=NC*TS(IEL)*EL/2 0D0
      F(IA,1)=F(IA,1)+FE
      F(IB,1)=F(IB,1)+FE
  103 CONTINUE
      RETURN
      END
      SUBROUTINE BANDEC(NEQ,MAXB,NVEC)
      IMPLICIT REAL*8(A-H,O-Z)
      COMMON/PORD/X(200),Y(200),EZERO,BVIN,THICK,TALFA,APS
      COMMON/MAFO/A(200,50),F(200,1),H(200),TS(200),TSAT,CK,NEL,NSNP,N^
BA
     *N,ICOR(200,3)
      LOOP=NEQ-1
      DO 201 I=1,LOOP
      MB=I+1
      NB=MIN0(I+MAXB-1,NEQ)
      DO 201 J=MB,NB
      L=J+2-MB
      D=A(I,L)/A(I,1)
      DO 202 MM=1,NVEC
  202 F(J,MM)=F(J,MM)-D*F(I,MM)
      MM=MIN0(MAXB-L+1,NEQ-J+1)
      DO 201 K=1,MM
      NN=L+K-1
  201 A(J,K)=A(J,K)-D*A(I,NN)
      DO 203 I=1,NVEC
  203 F(NEQ,I)=F(NEQ,I)/A(NEQ,1)
      DO 204 I=2,NEQ
      J=NEQ-I+1
      K=MIN0(NEQ-J+1,MAXB)
      DO 204 MM=1,NVEC
```

```
      DO 205 L=2,K
      MB=J+L-1
205   F(J,MM)=F(J,MM)-A(J,L)*F(MB,MM)
204   F(J,MM)=F(J,MM)/A(J,1)
      RETURN
      END
```

BIBLIOGRAPHY

1. Ballback, L. J., The Operation of a Rotating Wickless Heat Pipe, M. S. Thesis, Naval Postgraduate School, Monterey, California, December 1969.

2. Kutateladze, S. C., On the Transition to Film Boiling Under Natural Convection, Kotloturbostroenie, No. 3, pp. 10, 1948.

3. Sakhuja, R. K., Flooding Constraint in Wickless Heat Pipes, ASME Paper No. 73-WA/HT-7.

4. Chaiyuth Tantrakul, Condensation Heat Transfer Inside Rotating Heat Pipe, M. S. and M. E. Thesis, Naval Postgraduate School, Monterey, California, June 1977.

5. Schafer, C. E., Augmenting the Heat Transfer Performance of Rotating, Two-Phase Thermosyphons, M. S. Thesis, Naval Postgraduate School, Monterey, California, December 1972.

6. Corley, R. D., Heat Transfer Analysis of a Rotating Heat Pipe Containing Internal Axial Fins, M. S. Thesis, Naval Postgraduate School, Monterey, California, June 1976.

7. Lew, G. T., A Three-Dimensional Solution of the Transient Field Problem Using Isoparametric Finite Elements, M. S. Thesis, Naval Postgraduate School, Monterey, California, December 1972.

8. Sparrow, E. M., and Gregg, J. L., A Theory of Rotating Condensation, Journal of Heat Transfer, Vol. 81 Series C, pp. 113-120, May 1959.

9. Huebner, K. H., The Finite Element Method For Engineers, John Wiley & Sons, 1974.

10. Segerlind, L. J., Applied Finite Element Analysis, John Wiley & Sons, 1976.

INITIAL DISTRIBUTION LIST

		No. Copies
1.	Defense Documentation Center Cameron Station Alexandria, Virginia 22314	2
2.	Library, Code 0142 Naval Postgraduate School Monterey, California 93940	2
3.	Department of Mechanical Engineering Code 69 Naval Postgraduate School Monterey, California 93940	1
4.	Dr. P. J. Marto, Code 69 Department of Mechanical Engineering Naval Postgraduate School Monterey, California 93940	1
5.	Dr. David Salinas, Code 69Zc Department of Mechanical Engineering Naval Postgraduate School Monterey, California 93940	1
6.	Indonesian Naval Institute of Technology PUSDIK IAL/SESKOAL Cipulir Kebayoran Lama Jacarta, Indonesia	1
7.	Dr. Diran Department of Mechanical Engineering Bandung Institute of Technology Jalan Ganesa Bandung, Indonesia	1
8.	Major Purnomo, I. S. KORESUMAT TNI-AD Jalan Ternate 8 Bandung, Indonesia	2